

# Selective photocatalytic and photoelectrocatalytic synthesis of valuable compounds in aqueous medium

Marianna Bellardita<sup>1\*</sup>, Vittorio Loddo<sup>1</sup>, Vincenzo Augugliaro<sup>1</sup>, Leonardo Palmisano<sup>1</sup>, Sedat Yurdakal<sup>2\*</sup>

<sup>1</sup>Engineering Department, University of Palermo, Viale delle Scienze Ed. 6, 90128, Palermo, Italy.

<sup>2</sup>Department of Metallurgical and Materials Engineering, Faculty of Engineering, Dokuz Eylül University, Tınaztepe Campus, Buca, 35390 İzmir, Türkiye.

Corresponding authors: Marianna Bellardita ([marianna.bellardita@unipa.it](mailto:marianna.bellardita@unipa.it)), Sedat Yurdakal ([sedat.yurdakal@deu.edu.tr](mailto:sedat.yurdakal@deu.edu.tr))

## Abstract

In the past decades, photocatalytic and photoelectrocatalytic methods have been widely employed for the degradation of harmful compounds present both in gaseous and aqueous effluents. In the last years scientists have paid great attention to the synthesis of valuable compounds and hydrogen production. Organic syntheses are generally carried out in organic solvents, under high temperature/pressure, with toxic oxidants such as permanganate. On the other hand, photocatalysis and photoelectrocatalysis using water as solvent, air or water as oxidant, and sunlight as energy source, can be an efficient alternative to the traditional, non-environmentally friendly methods. This review summarizes the photocatalytic and photoelectrocatalytic transformations of organic molecules to commercially valuable products in water, sometimes evaluating also the contemporary H<sub>2</sub> production. The reaction conditions, mechanisms and kinetics will be presented and discussed. Future perspectives will also be given.

**Keywords:** Selective photocatalytic syntheses; Selective photoelectrocatalytic syntheses; Biomass photoreforming; High added value chemicals; H<sub>2</sub> production; Green syntheses

## 1. Introduction

Heterogeneous photocatalysis (PC) technology is based on the ability of some solids called photocatalysts, which have typical semiconductor properties to generate pairs of electrons (e<sup>-</sup>) and positive holes (h<sup>+</sup>) when irradiated by light of appropriate energy [1–3]. These e<sup>-</sup>/h<sup>+</sup> couples can induce, directly or indirectly through the formation of radicals, oxidation and reduction reactions involving the species adsorbed on the surface of the semiconductor solid.

Heterogeneous photocatalysis was generally used until a few years ago in the field of degradation of organic polluting species present in aqueous and gaseous effluents, even if the reactions studied almost never had industrial application [4–6]. More recently, researchers expert in this technology have turned towards the synthesis of some molecules with high added value [7–11], such as the partial oxidation of alcohols to aldehydes [12–15], reduction reactions [16–19], biomass conversion [7,20–23], C-C bond breaking [24,25], CO<sub>2</sub> activation [26–29] and H<sub>2</sub> formation [30–35].

Despite the fact that the photocatalytic method is very versatile for many types of reactions, it has some drawbacks. Among the most important we mention the low exploitation of solar energy which is due to the too high band-gap values of the photocatalysts and the not very significant efficiency which is due to the high recombination rate of the photogenerated e<sup>-</sup>/h<sup>+</sup> charges.

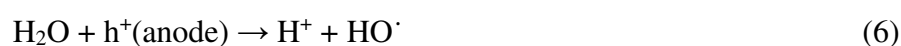
Electrocatalysis represents a more cost-effective process as the redox reactions occur in an electrochemical cell where the electrocatalyst lowers the overpotential of the reactions allowing a direct conversion of electric energy into chemical one.

This technology also has some drawbacks such as low selectivity towards the product(s), high overpotential values for some reactions, and often poor Faradaic efficiency. The low selectivity and high overpotential values may depend on significant adsorption energies of some intermediates of the reaction, while the low Faradaic efficiency may depend on competitive reactions that are kinetically favored, and more generally it can be said to parasitic processes.

An important possibility to improve process efficiency is to use different approaches that show synergistic effects. For example, the photocatalytic and electrochemical methods can be used in tandem, i.e. coupled. In this case we will talk about photoelectrocatalysis (PEC), and some systems of this type reported in the literature will be presented in the second part of this review. The performance of the first process can be improved if an external bias is applied to a photoelectrode with a catalyst supported in various ways [36–39]. The fundamental principle on which this configuration is based is to obtain greater effectiveness in the separation of the e<sup>-</sup>/h<sup>+</sup> pairs photogenerated as a result of light irradiation. In other words, their lifetime is increased, making them more available to induce oxidation and reduction reactions.

Differently from photocatalysis, the PEC method requires an external bias to be applied to a thin semiconductor plate on conductive support [40]. Fluorine doped tin oxide (FTO), indium tin oxide (ITO) glasses or metal plates could be used as conductive supports, therefore there are no separation problems of the catalyst from the reaction medium.

In the field of organic syntheses in the presence of water as the solvent, the low conversion and selectivity towards the target compounds obtained by the photocatalytic method, as above reported, can be enhanced by PEC thanks to the spatial separation of the oxidation and reduction processes at the two electrodes [38,41,42]. In fact, as the hole will proceed to the anode for the oxidation reaction and the electron will move to the cathode for the reduction reaction, the efficiency of the reaction examined increases compared to photocatalysis and electrocatalysis. The main reaction mechanism of the produced radical species ( $O_2^{\cdot-}$ ,  $HO_2^{\cdot}$ ,  $HO^{\cdot}$ , and  $h^+$ ) on cathode and anode surfaces in aerobic condition is reported below (Eqn. 1-6). Oxygen is an electron trap in aerobic condition at cathode surface.



The choice of materials to be used for the electrodes must be made taking into account the oxidation and reduction potentials of the substrates used to address the selectivity towards the desired products [43].

In this review, we give an overview of the partial oxidation reactions via photocatalysis and photoelectrocatalysis only in the presence of water as the solvent. The reactions were divided into categories of starting compounds and particular attention was paid to the materials used and the experimental conditions for each specific reaction. It is hoped that this review can help to choose the most suitable photo/photoelectro-catalytic systems for each specific synthesis process.

## 2. Photocatalytic partial oxidation reactions

### 2.1 Partial photocatalytic oxidation of alcohols to aldehydes

In these last years, studies were carried out on the feasibility of alcohol partial oxidation to the corresponding aldehydes by photocatalysis in organic-free water. G. Palmisano et al. [44] studied the formation of 4-methoxybenzaldehyde (p-anisaldehyde, PAA, a compound used for

confectioneries and beverages) from the photocatalytic selective oxidation of 4-methoxybenzyl alcohol, 4-MBA. The process was carried out in a batch reactor containing aqueous suspensions of commercial and home-prepared TiO<sub>2</sub> [45]; the results highlighted that the mechanism of 4-MBA disappearance consisted of two different reaction pathways occurring in parallel, i.e. the partial oxidation to PAA and the total oxidation to CO<sub>2</sub>. The home-prepared anatase based photocatalysts were obtained under mild conditions and showed to be much more selective than the commercial ones, i.e. TiO<sub>2</sub> Merck and Degussa P25, with a selectivity towards PAA of ca. 41% and a conversion of 65%. Notably, a maximum selectivity towards PAA of ca. 56% (i.e. ca. 3 times higher than that obtained with commercial TiO<sub>2</sub>) was achieved by using a home-prepared uncalcined brookite TiO<sub>2</sub>, used for the first time for synthetic purposes [46].

Augugliaro et al. [47] used home prepared TiO<sub>2</sub> rutile catalysts, obtained at room temperature, by a new sol-gel route starting from TiCl<sub>4</sub> as the Ti precursor for the partial oxidation of benzyl alcohol (BA) and 4-MBA. The highest selectivity towards the corresponding aldehydes for both alcohols was found with a poor crystallized TiO<sub>2</sub> rutile prepared at 333 K. The selectivity was not affected by the reaction-rate value and adsorption played a major role. Indeed, it was found that the extent of PAA adsorption was negligible with respect to that of benzaldehyde (BAD) (23%). Consequently, the different selectivity towards BAD and PAA (38 vs 60%) can be justified by considering the very different adsorption extent of the two aldehydes. Successively, room temperature home-made rutile was tested for the partial oxidation of different aromatic alcohols in water suspensions [48]. In addition to the partial oxidation of MBA to PAA, the photocatalytic oxidation of some 4-substituted benzyl alcohols to the corresponding aldehydes was carried out; i.e. benzyl alcohol (BA) to benzaldehyde (BAD), 4-methylbenzyl alcohol (MeBA) to 4-methylbenzaldehyde (MeBAD) and 4-nitrobenzyl alcohol (4-NBA) to 4-nitrobenzaldehyde (4-NBAD). Selectivity values as high as 74% were obtained and home prepared samples were more active than commercial ones. The effect of the aromatic alcohol substituent on the partial oxidation performance was in accord with the Hammett's relationship. Low crystalline home prepared rutile was also efficient for the partial oxidation of piperonyl alcohol to piperonal under environmentally friendly conditions [10]. Di Paola et al. [49] compared the activity of two commercial and two home prepared TiO<sub>2</sub> powders for the partial oxidation of 4-MBA under UV light irradiation. The crystallinity degree and the OH surface density influenced the photocatalytic performance, and the least crystalline and most hydroxylated home-made samples exhibited the highest selectivity toward PAA. The oxidant power was reduced, although the high density of surface OH, because those belonging to amorphous part of TiO<sub>2</sub> surface were not able to be transformed into radicals under irradiation,

and consequently the partial oxidation was favoured. EPR analyses showed, in fact, that the amount of HO· radicals formed under irradiation was not directly linked to the total number of surface hydroxyl radicals.

Yurdakal et al. [50], investigated the influence of N-doping TiO<sub>2</sub> on selectivity of photocatalytic oxidation of 4-MBA towards PAA in water under simulated solar irradiation. The results indicated that the doping with nitrogen and the exploitation of solar light, were beneficial for increasing the selectivity of the partial oxidation of 4-MBA to PAA. In particular, poorly crystalline catalysts, prepared by using NH<sub>4</sub>Cl as nitrogen source, were found to be the most selective samples, by reaching a 90% selectivity under simulated solar light irradiation.

The influence of the addition of different metal species in TiO<sub>2</sub> photocatalysts for the partial oxidation of aromatic alcohols was studied by Bellardita et al. [13]. The substrates were benzyl alcohol (BA), 4-methoxybenzyl alcohol (4-MBA), and 4-hydroxybenzyl alcohol (4-HBA). The metals used to modify the TiO<sub>2</sub> were, Cu, Ni, Nb, Ce, W and Mg. The presence of Nb and W species was beneficial, and high selectivity was found with conversions greater than 30%. For the other metals a significant reduction in conversion was achieved compared to bare TiO<sub>2</sub>. The metals probably modify some of the surface properties, such as the distribution and type of acidic and basic sites. Table 1 shows the results obtained.

**Table 1:** Alcohol conversion (X) and selectivity to the corresponding aldehyde (S) in the presence of the different catalysts. Note that the symbol of metal in the acronyms indicates the presence of metal species, i.e. metal in some oxidized form(s), not zerovalent metals.

Sample	BA		4-MBA		4-HBA	
	X	S	X	S	X	S
TiO <sub>2</sub>	23	19	32	41	24	10
TiO <sub>2</sub> -Ni	3	75	7	94	11	7
TiO <sub>2</sub> -Nb	36	20	36	75	16	32
TiO <sub>2</sub> -Ce	18	19	10	100	10	30
TiO <sub>2</sub> -Cu	15	19	6	100	8	16
TiO <sub>2</sub> -W	37	25	32	91	33	17
TiO <sub>2</sub> -Mg	8	90	29	67	26	10

One of the parameters influencing the photocatalytic activity recently investigated is the presence or the prevalence of a specific TiO<sub>2</sub> facet that can address both the substrate conversion and the selectivity towards target compounds [51–56]. Bellardita et al. [51] found that the partial oxidation of 4-MBA was less influenced by the presence of specific TiO<sub>2</sub> facets, and the presence of residual fluorine played a major role. Furthermore, the simultaneous presence of more than one facet is beneficial due the formation of an efficient heterojunction between facets exhibiting different energy values of the respectively conduction and valence band edges.

Yurdakal et al. [14] compared the partial oxidation of 2-hydroxybenzyl alcohol and 4-hydroxybenzyl alcohol by using different TiO<sub>2</sub> based photocatalysts by varying the solution pH in the range 3-11. The highest activity was obtained at pH = 11 by using high crystalline TiO<sub>2</sub> samples. The selectivity towards the corresponding aldehyde and acid was higher for 4-hydroxybenzyl alcohol than for 2-hydroxybenzyl alcohol due to the less tendency of the first substrate to the complete mineralization. FT-IR spectroscopy under in situ UV irradiation revealed that 2-hydroxybenzyl alcohol is strongly adsorbed on the TiO<sub>2</sub> surface in a bidentate way, while 4-hydroxybenzyl alcohol is adsorbed weaklier in monodentate way [57].

TiO<sub>2</sub> particles loaded with WO<sub>3</sub> (WO<sub>3</sub>/TiO<sub>2</sub>), synthesized by impregnation of tungstic acid followed by calcination, were used for photocatalytic oxidation of alcohols in water with molecular oxygen under irradiation at  $\lambda > 350$  nm by Tsukamoto et al. [58]. WO<sub>3</sub>/TiO<sub>2</sub> system successfully promoted the selective production of aldehydes with higher catalytic activity than pure TiO<sub>2</sub>. The results showed that with a percentage of W of 7.6, a high catalytic activity for benzyl alcohol partial oxidation with selectivity towards aldehyde much higher than the previously reported photocatalytic systems (56%) was observed. This behaviour was probably due to the electron transfer from the conduction band of TiO<sub>2</sub> to the WO<sub>3</sub> surface. This generates a charge separation of electron and holes pairs thus increasing the system efficiency.

Recently, several attempts have been devoted to the development of structured spinels such as CuBi<sub>2</sub>O<sub>4</sub> to be used not only as photocatalysts for the degradation of pollutants, but also for the partial oxidation of alcohols. Bellardita et al. [59], demonstrated the effect of the coexistence of CuBi<sub>2</sub>O<sub>4</sub> (CBO) and TiO<sub>2</sub> in the selective photocatalytic oxidation of 4-MBA under simulated solar light irradiation by using water as the solvent. The hetero-catalysts having different mass ratios were prepared by an inexpensive, easy and reproducible ball milling method. The sample 4%CBO/HP-TiO<sub>2</sub> 150 rpm (the rotation speed of the ball mill), showed the highest photoactivity with an alcohol conversion of 77%, a selectivity towards aldehyde of 45% and a yield of 35% after 4 h irradiation.

Li et al. [60] carried out the partial oxidation of benzyl alcohols and the simultaneous production of H<sub>2</sub> by using a combination of a ruthenium molecular catalyst and platinum particle modified graphitic carbon nitride (Pt-g-C<sub>3</sub>N<sub>4</sub>) as the photocatalyst irradiated by visible light. The incorporation of Ru consistently improved the selectivity (over 99%) towards aldehydes, probably due to the formation of highly active Ru(IV) intermediates. Moreover, UV-vis and PL spectroscopy evidenced that the photogenerated holes were transferred mainly from the carbon nitride to the molecular catalyst rather than to the substrate, thus initiating a metal-based selective oxidation.

Phosphorus doped home prepared g-C<sub>3</sub>N<sub>4</sub> photocatalysts showed high activity both under UV irradiation and simulated sunlight towards the selective oxidation of benzyl alcohol, 4-methoxy benzyl alcohol and piperonyl alcohol (PA) in aqueous medium, reaching selectivity values up to 100% for BA and 4-MBA and of 46 % for PA [61]. The activity of the home prepared g-C<sub>3</sub>N<sub>4</sub> was higher than that of commercial home-prepared (HP) and commercial (P25) TiO<sub>2</sub> samples (Table 2). The different conversion degree of the three alcohols (4-MBA > PA > BA) indicates that with both photocatalysts the presence of the oxy-substituent in the aromatic ring favours the alcohol partial oxidation.

**Table 2:** Alcohols conversion and selectivity towards aldehydes in the presence of C<sub>3</sub>N<sub>4</sub> and TiO<sub>2</sub> samples after 4 h of UV or simulated solar light irradiation.

Sample	BA				4-MBA				PA			
	UV		Vis		UV		Vis		UV		Vis	
	X	S	X	S	X	S	X	S	X	S	X	S
g-C <sub>3</sub> N <sub>4</sub>	33	56	20	51	100	64	100	72	36	21	25	24
P25	15	23	13	12	18	35	18	23	12	21	12	24
HP	7	37	5	23	27	49	20	56	18	22	10	22

The photocatalytic synthesis of vanillin was carried out by Sampaio et al. [62] under UV-LED irradiation starting from vanillyl alcohol by using ZnO and hybrid materials containing different amounts of nitrogen doped carbon nanotubes (N-CNT) as the catalysts. The presence of the carbon phase in the composite materials (from 5.0 to 10 wt.%) revealed to be crucial for increasing the performance of the photocatalysts. The best results for vanillyl alcohol oxidation was obtained using the composite containing 5% of carbon phase (5.0%N-CNT/ZnO), obtaining an increase of 22% in vanillin concentration with respect to bare ZnO after 2 h of reaction.

A remarkable conversion of vanillyl alcohol equal to 66.9% with a selectivity of 77.8% and a yield of 52.1% in vanillin, coupled with H<sub>2</sub> evolution, was obtained by Du et. al. [63]. They

prepared NiS/Cd<sub>0.6</sub>Zn<sub>0.4</sub>S bifunctional catalysts by a one pot hydrothermal technique for a sunlight driven reaction. The optimal conditions were 8% NiS/Cd<sub>0.6</sub>Zn<sub>0.4</sub>S. The main factor responsible for improving the photocatalytic performance is the formation of a Schottky junction between NiS and Cd<sub>0.6</sub>Zn<sub>0.4</sub>S, in which NiS act as a co-catalyst contributing to the separation, transfer, and utilization of the photoinduced carriers.

The almost complete oxidation of aromatic alcohols to the corresponding aldehydes in aqueous suspension irradiated by a LED was obtained by Tanaka et al. [64] in the presence of a photocatalyst formed by gold nanoparticles supported on cerium oxide (Au/CeO<sub>2</sub>). The photocatalyst exhibited a strong absorption at around 550 nm due to surface plasmon resonance (SPR) for which an electron transfer from Au nanoparticles to the semiconductor occurred under visible light irradiation.

## **2.2 Biomass derivatives**

In the last years natural biomass is deemed a promising alternative energy source with a zero-greenhouse impact to petroleum derivatives [65]. Extensive investigations have been carried out to boost the use of biomass as feedstock to produce fine chemicals, intermediates for the synthesis of platform molecules and fuels [7,21,65–67]. For this purpose, photocatalytic reforming has emerged as a new process contemporary allowing the biomass valorization with the formation of high added value chemical and H<sub>2</sub> (Figure 1) [8,19,23,68–71]. Photocatalytic H<sub>2</sub> formation by water splitting, although in principle is the most desirable process, remains a challenge because its efficiency is poor due to the high recombination rate of the photoproducted charges and to thermodynamic issues. Nevertheless, the addition of organic sacrificial compounds, reacting with holes, not only makes electrons more easily available for the reduction of H<sup>+</sup> ions, but also decreases the thermodynamic barrier of water splitting, as observed for the first time by Kawai and Sakata [72].

In this section we focused on the partial oxidation, sometimes coupled with the production of H<sub>2</sub>, of the main biomass components such as lignocellulose, glycerol, carbohydrates (mainly glucose and fructose) and 5-hydroxymethyl-2-furfural (HMF), that represents a target compound deriving from partial conversion of biomass derivatives because it can be used as the starting substrate for the production of more valuable chemicals of industrial interest [73,74].



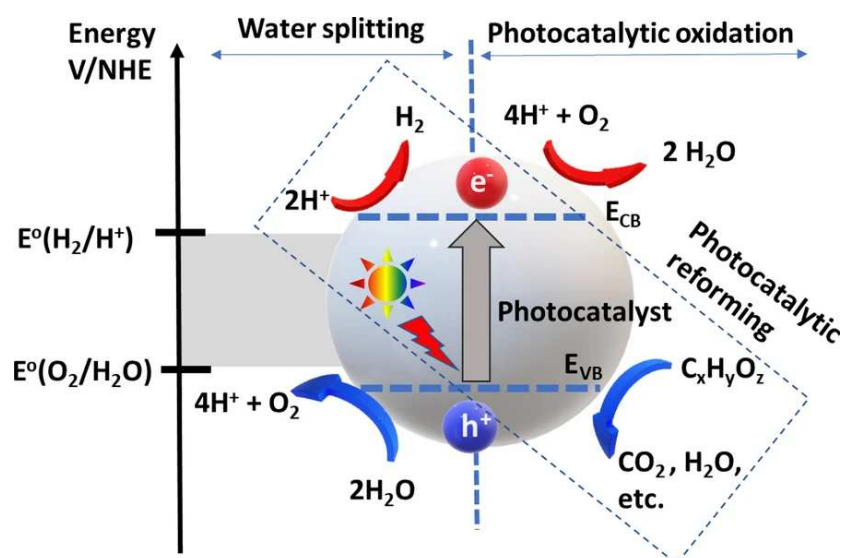


**Figure 1** Illustration of water splitting and biomass photocatalytic oxidation under light irradiation [71].

### 2.2.1 Lignocellulose

The name lignocellulose refers to biomass derivatives rich in cellulose such as hemicellulose and lignin. Although it is widely available, its complex chemical composition does not make it easy to use due to the multiplicity of compounds that can be formed and the consequently complexity of the separation process. Moreover, to enhance both conversion and selectivity towards target compounds, organic solvents have been frequently used and few are the works in which pure water is used as the solvent. Lu et al. [75] performed the photocatalytic depolymerization of rice husk in  $\text{H}_2\text{O}_2$  aqueous solution by using  $\text{TiO}_2$  under UV irradiation and obtained 172 different organic compounds. The most abundant components were alkanes, ketones and phthalates.

$\text{Ag-AgCl/ZnO}$  nanorods allowed 100% of lignin degradation to methane and biogas under solar light irradiation [76]. Zero valent Bi and Pt species on the  $\text{TiO}_2$  surface were effective in the conversion (ca. 84 % after 1h) of lignin under solar light illumination [77]. The main identified partial oxidation compounds were vanillic acid, guaiacol, vanillin and 4-phenyl-1-buten-4-ol and their amount depended on the Bi/Pt ratio and pH.

Srisasiwimon et al. [78] used lignin both as natural carbon source in the preparation of  $\text{TiO}_2$  based photocatalysts and as a raw precursor of valuables compounds. The sample  $\text{TiO}_2/\text{lignin}$  1:0.5 showed the highest activity under UV-A irradiation with a lignin conversion of ca. 40% and a vanillin yield of 1.68% after 3h of irradiation.

A more efficient use of lignocellulosic biomass is the photoreforming for H<sub>2</sub> production [79–82]. CdS/CdO<sub>x</sub> photocatalysts were effective for visible light photoreforming of cellulose, hemicellulose and lignin to H<sub>2</sub> at room temperature in alkaline aqueous solution [80].

By coupling photocatalysis with acid hydrolysis under anaerobic conditions using UV irradiation, it was possible to contemporarily obtain H<sub>2</sub>, carbohydrates and little amount of 5-hydroxymethylfurfural [82]. The main identified valuable chemicals obtained in the liquid phase were erythrose, arabinone and HMF in addition with H<sub>2</sub> in the gas phase. After 10 h of irradiation the cellulose conversion efficiency was 66%, the H<sub>2</sub> yield 123 μmol in 0.6M H<sub>2</sub>SO<sub>4</sub>, and the HMF, erythrose and arabinone yields were 12.8%, 5.4% and 3.3%, respectively. In Figure 2A the hypothesized pathway of cellulose decomposition is reported. Speltini et al. [83] irradiated an aqueous cellulose suspension by UV-A or sunlight in the presence of Pt/TiO<sub>2</sub> as the photocatalyst. Among the formed products glucose and HMF were identified (Figure 2B) that gave rise subsequently to the photoreforming process by favouring H<sub>2</sub> production. Moreover, the formation of coloured compounds deriving from HMF induced an “in situ dye sensitization” that allowed the exploitation of solar light.

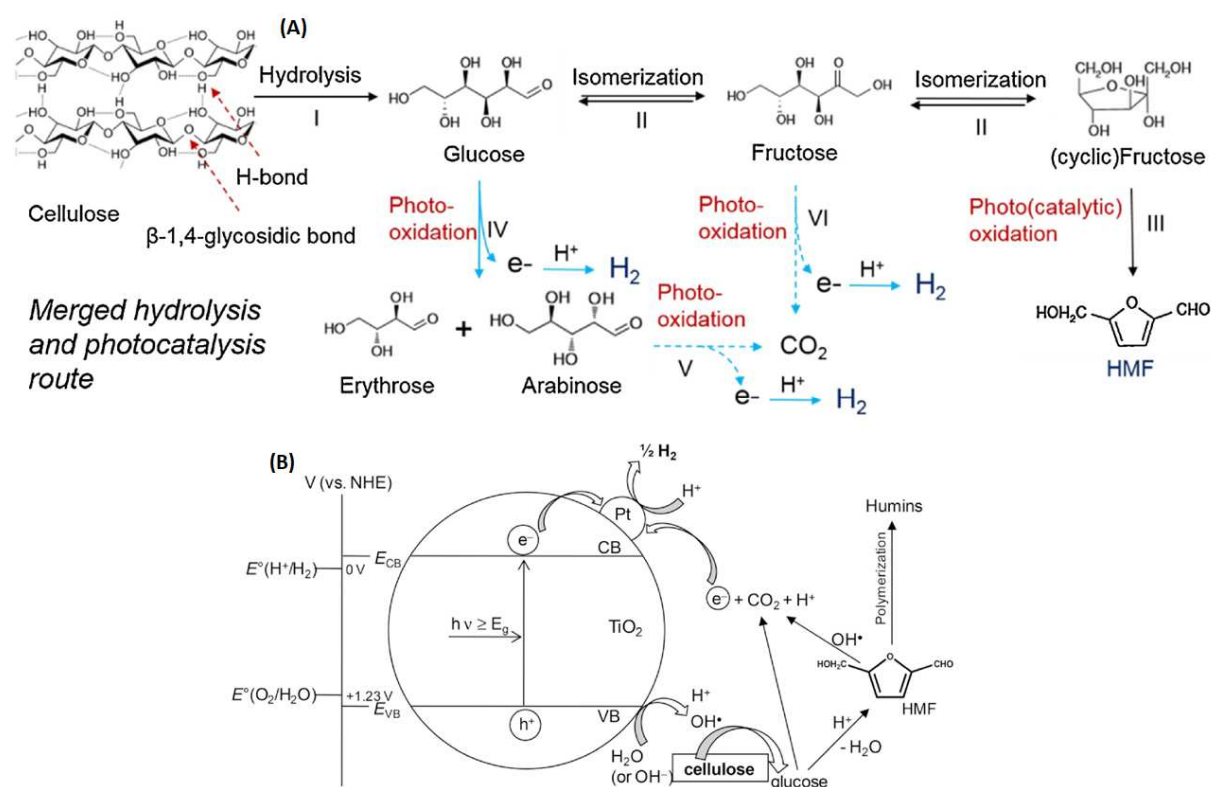


**Figure 2** Hypothesized pathway of the decomposition of cellulose decomposition by coupling heterogeneous photocatalysis with acid hydrolysis (A) [82] and lignin degradation mechanism in the presence of Pt-TiO<sub>2</sub> photocatalysts (B) [83].

NiO<sub>x</sub> modified with graphitic carbon layers deriving from glucose was coupled with TiO<sub>2</sub> (TiO<sub>2</sub>/NiO<sub>x</sub>@Cg) and used for the photoreforming of cellulose aqueous solution, both at room temperature and 80°C by using a 500-W Xe lamp as the irradiation source [81]. The H<sub>2</sub> production rate was 270 μmol h<sup>-1</sup>g<sup>-1</sup> and 4000 μmol h<sup>-1</sup> g<sup>-1</sup> at room temperature and 80°C, respectively.

NiS/CdS composites allowed to achieve an apparent quantum efficiency of 44.9% with a H<sub>2</sub> production rate of 1512.4 μmol h<sup>-1</sup> g<sup>-1</sup> from lignin and lactic acid aqueous solution [84]. The high activity was attributed to an effective heterojunction between the two components allowing an efficient charge separation and, consequently, a longer charge carrier lifetime.

### **2.2.2 Glycerol**

Glycerol is available in large quantities as it is a byproduct of biodiesel and fats manufacturing that can become an economic resource by its valorisation as precursor for the synthesis of value-added chemicals [85]. In particular, glyceraldehyde (GAD) and 1,3-dihydroxyacetone (DHA) find applications in the fine chemical, cosmetic, pharmaceutical and food industries [86]. As glycerol contains three hydroxyl groups almost equivalent as regards adsorption and chemical reactivity, its selective oxidation is complex and generally low conversion and selectivity values have been obtained. However, glycerol adsorption mode [87] and produced radical species [88] play an essential role and depend on the used catalysts.

We have focused only on the papers in which the partial oxidation of glycerol is reported, sometimes coupled with the contemporary production of H<sub>2</sub> (photoreforming) and we have left out those in which only the formation of H<sub>2</sub> is considered.

Maurino et al. [89] investigated the photocatalytic conversion of glycerol by using two commercial TiO<sub>2</sub> samples (P25 and Merck) as photocatalysts in aqueous solutions. The influence of surface fluorination of the powders, pH of the solution and glycerol concentration were studied. Glyceraldehyde (GAD) and 1,3-dihydroxyacetone (DHA) were the main partial oxidation compounds formed. The two photocatalysts showed a different activity having been observed a different conversion rate and selectivity degree, and the fluorination of the surface had a positive effect on both powders reducing the glycerol oxidation rate and enhancing the intermediates production, but a more prominent effect was observed for P25. Starting from an initial glycerol concentration of 1 mM and F-P25, the glycerol conversion was less than 30% and an almost 100% selectivity towards DHA was obtained while GAD was also produced starting from higher substrate concentrations.

By using both commercial and home-made TiO<sub>2</sub> based photocatalyst under aerobic conditions and UV irradiation, GAD, DHA, formic acid (FA), CO<sub>2</sub> and two unknown compounds were found in the aqueous solution by Augugliaro et al. [90]. Commercial TiO<sub>2</sub> P25 was the most active sample with a 35% glycerol conversion and a global selectivity towards the identified intermediated of ca. 45%.

Au<sub>x</sub>Cu-CuS@TiO<sub>2</sub> plasmonic heterostructures revealed high efficiency in the partial oxidation of glycerol under simulated solar light irradiation with a glycerol conversion of 72% and selectivity towards DHA of 66% [91]. Glyceric and glycolic acid were also formed in less amounts. The high activity is due both to formation of an efficient heterojunction between TiO<sub>2</sub> and Au<sub>x</sub>Cu alloy nanoparticles and the plasmonic resonance on the Au particles.

Limpachanangkul et al. [92] compared the activity of TiO<sub>2</sub>, SiC, Bi<sub>2</sub>O<sub>3</sub> and ZnO for the conversion of glycerol to value added compounds in aqueous solution in the presence of H<sub>2</sub>O<sub>2</sub> as electron acceptor under UV light irradiation. The activity of SiC, Bi<sub>2</sub>O<sub>3</sub> and ZnO were higher than that of TiO<sub>2</sub>, and an almost total conversion of glycerol was achieved in 8h. With all of the photocatalysts the same products (dihydroxyacetone, glyceraldehyde, glyceric acid, formic acid and glycolic acid) were obtained. Interestingly, glyoxylic acid was also formed in the presence of Bi<sub>2</sub>O<sub>3</sub>.

Flower-like BiWO<sub>6</sub> samples were used as visible-light photocatalysts alternative to TiO<sub>2</sub> for aerobic partial oxidation of glycerol in aqueous solution at room temperature [93]. The samples resulted very selective towards DHA being the selectivity higher than 90% with a glycerol conversion of 96% after 5h of irradiation. Zhang et al. [94] used silica-entrapped Bi<sub>2</sub>WO<sub>6</sub> photocatalysts for the selective conversion of glycerol under green conditions affording a conversion of 40% after 8h of visible light irradiation, with a selectivity of 94% and 6% towards DHA and GHA, respectively. A similar behaviour was noticed in the presence of a Bi/Bi<sub>3.64</sub>Mo<sub>0.36</sub>O<sub>6.55</sub> heterostructure [95]. Also in this case DHA was the main product under solar light irradiation with a selectivity of ca. 87% at 42% after 4h of irradiation.

Chong et al. [96] carried out the photoreforming of glycerol aqueous solution by using a 300 W Xenon lamp as the light source in the presence of different M-TiO<sub>2</sub> (M: 0.1 wt% Pt, Rh, Pd, Au, Ru, 1 wt% Cu,Ni) polymorphs exposing different facets. The main intermediates were hydroxyacetaldehyde, GAD, FA and formaldehyde in the liquid phase and H<sub>2</sub> in the gas phase. Rutile exposing prevalently the {110} facet was highly selective towards hydroxyacetaldehyde (selectivity up to 96% with a conversion of ca. 20%) whilst in the presence of anatase exhibiting the {001} or {101} facets only 16% and 49% of hydroxyacetaldehyde was obtained. These

findings have been attributed to the higher formation of peroxo species onto the rutile surface and HO<sup>•</sup> radicals on the anatase surface.

The addition of metal species had no influence on the partial oxidation compounds formation, but it was essential for H<sub>2</sub> production, with the highest production rate (ca. 3000 μmol h<sup>-1</sup> g<sup>-1</sup>) observed in the presence of Pt.

Maslova et al. [97] studied glycerol photoreforming under simulated solar light irradiation by using different TiO<sub>2</sub> based commercial (P25 and DT-51) and laboratory prepared (Anatase=TiO<sub>2</sub>-m\_A and Rutile = TiO<sub>2</sub>-m\_R) photocatalysts on which Pt was photodeposited. Naked TiO<sub>2</sub>-m\_R was the most active sample towards H<sub>2</sub> production, and the activity order changed after Pt deposition being Pt-P25 the most efficient sample. Regarding the partial oxidation products, anatase resulted more selective towards GAD and rutile towards glycolaldehyde favoring the direct C–C cleavage.

The same research group [98] evaluated the activity of Pt hydrogenated TiO<sub>2</sub> towards the production of glycerol and high added value chemicals starting from glycerol solution under simulated solar light irradiation. In the liquid phase GAD, glycolaldehyde and FA were detected while H<sub>2</sub> and trace amounts of CO<sub>2</sub>, CO and CH<sub>4</sub> were noticed in the gas phase. Glycerol conversion degree, selectivity towards GAD, and H<sub>2</sub> productivity enhanced with the increase of Pt(1%w) dispersion on TiO<sub>2</sub> surface, while a decrease was observed in the selectivity towards glycolaldehyde. This finding suggests that Pt not only reduces the e<sup>-</sup>/h<sup>+</sup> recombination rate and enhances the H<sub>2</sub> production but also affects the selectivity towards the partial oxidation compounds.

The activity of coupled Cu<sub>2</sub>O-P25 samples simply prepared by ball milling was compared to that of Pt-P25 catalysts under both UV and simulated solar irradiation for glucose photoreforming [70]. H<sub>2</sub> and CO<sub>2</sub> were produced in the gas phase while DHA and GAD were found in the liquid phase with all of the photocatalysts. Cu<sub>2</sub>O was effective in replacing Pt, the most active sample was 3%Cu<sub>2</sub>O-P25 affording 33% of glycerol conversion, 10.3% and 5.4% DHA and GAD selectivity, respectively, and producing a H<sub>2</sub> concentration of 1.01 mM (0.17 mmol h<sup>-1</sup> g<sup>-1</sup>) and a CO<sub>2</sub> concentration of 0.16 mM after 5 h of UV irradiation. In Figure 3 the results related to the runs carried out under simulated solar light irradiation with the samples Pt-P25 and 3%Cu<sub>2</sub>O-P25 are reported. With the sample 3%Cu<sub>2</sub>O-P25 a slightly lower glucose conversion with respect to that obtained with Pt-P25 was obtained in the face of a greater selectivity and CO<sub>2</sub> and H<sub>2</sub> amount. The good activity has been ascribed both to the formation of an efficient heterojunction between the two components and an energy level of the Cu<sub>2</sub>O conduction band edge favorable to H<sub>2</sub> production.

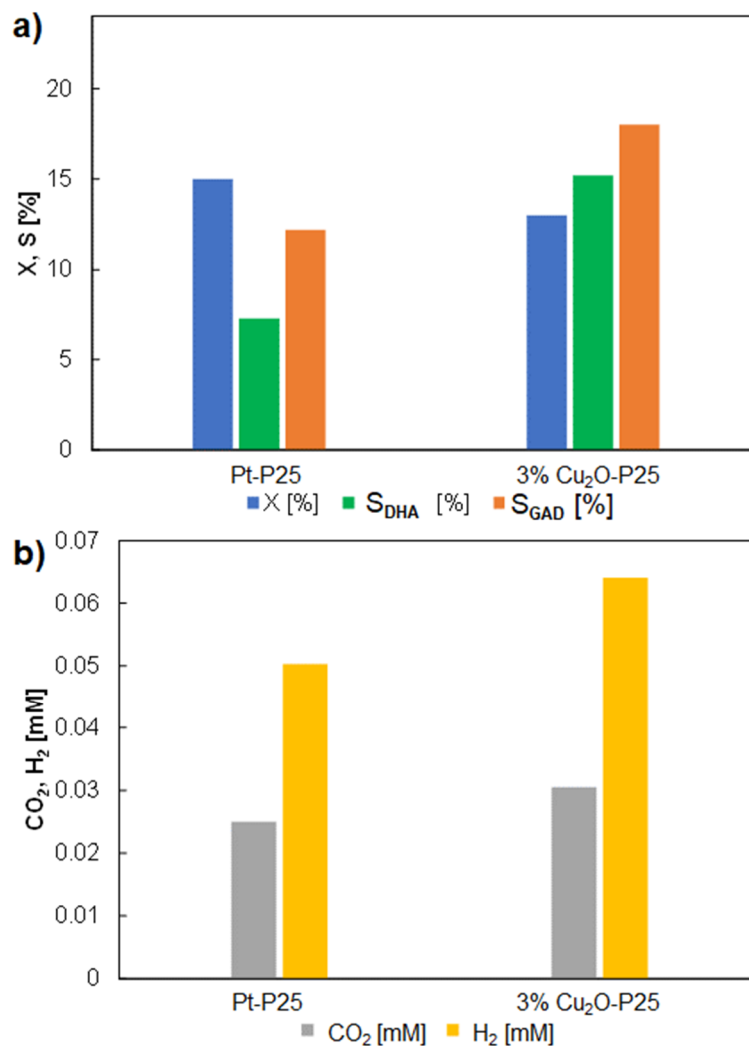


**Figure 3** a) Glycerol conversion (X), selectivity towards 1-3 dihydroxyacetone (S<sub>DHA</sub>), and glyceraldehyde (S<sub>GAD</sub>) and b) CO<sub>2</sub> and H<sub>2</sub> concentration [70].

1%Pt-Bi<sub>2</sub>WO<sub>6</sub> showed good activity as photocatalyst active under UV light in Ar deaerated aqueous solution for the reforming of glycerol. Formate was selectively formed (selectivity ca. 99%) along with H<sub>2</sub> (72 μmol g<sup>-1</sup> h<sup>-1</sup>) at pH=0 after 5h of irradiation.

### 2.2.3 Carbohydrates

Photoreforming of carbohydrates is particularly attractive as they are cheap and abundant biomass derivatives that constitute a renewable feedstock to produce valuable chemicals and H<sub>2</sub> (Figure 4).

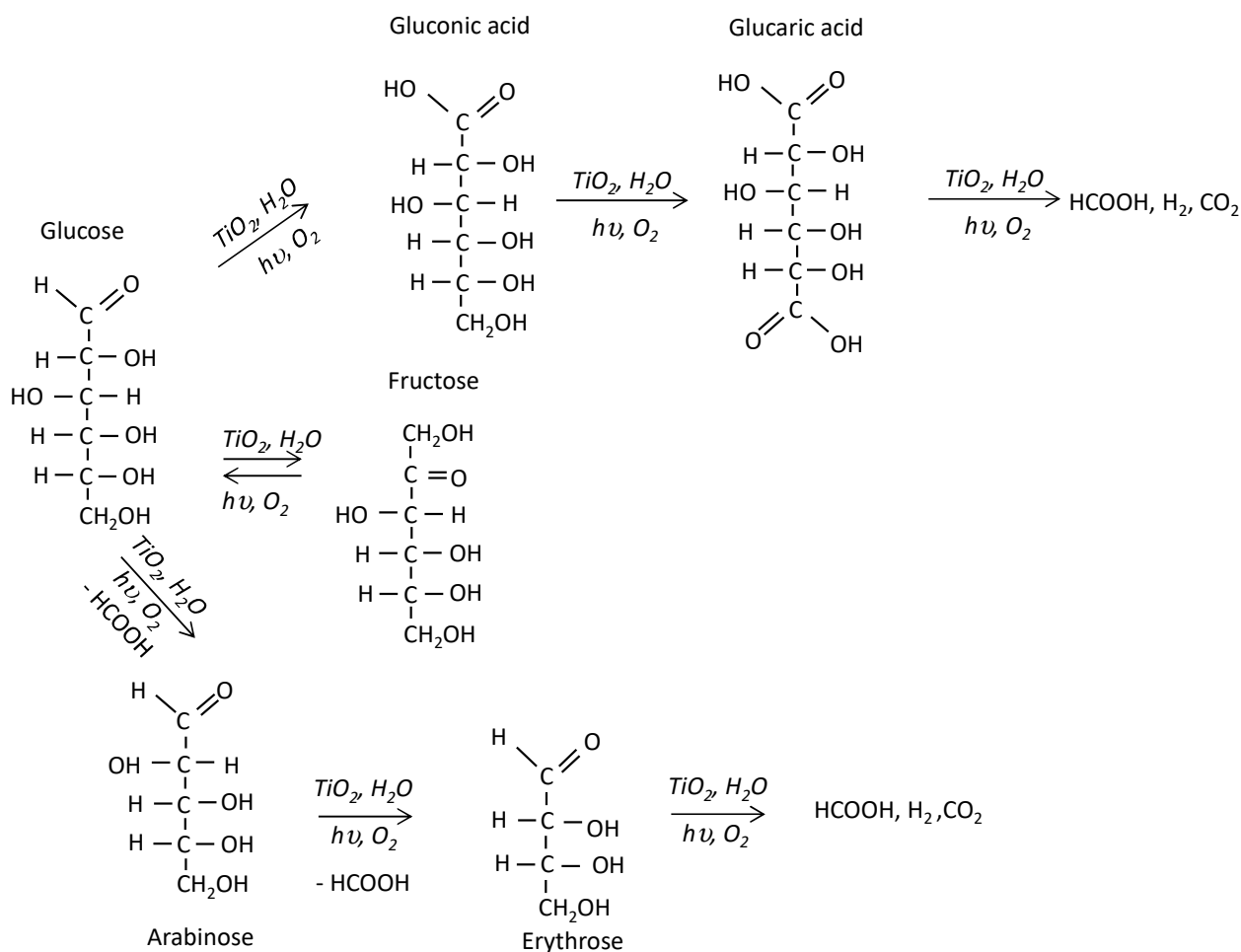


**Figure 4.** Hypothesized photocatalytic reaction pathway during glucose photoreforming [99].

Chong et al. [100] performed selective conversion of glucose to high value-added aldose in aqueous phase using Rh-TiO<sub>2</sub> based photocatalysts under simulated solar light irradiation. It was demonstrated that the photodegradation of glucose produced arabinose and erythrose involving initially the C1–C2 bond cleavage ( $\alpha$ -scission) (Figure 4). The total selectivity for the production of arabinose and erythrose on rutile TiO<sub>2</sub>-based photocatalyst was 91% at 65% conversion and a good H<sub>2</sub> amount was produced. Runs carried out in the presence of H<sub>2</sub>O<sub>2</sub> revealed that HO<sup>•</sup> radicals give rise to low selectivity, whilst peroxy species lead to high selectivity.

The visible-light mediated selective photo-oxidation of glucose using unmodified TiO<sub>2</sub> was studied by Da Vià et al. [101]. This photoactivation by visible light was achieved through the exploitation of a glucose-TiO<sub>2</sub> charge transfer complex whereby a metal-organic complex was formed with the reactant. Under the optimum conditions (catalyst to substrate ratio, lamp power and TiO<sub>2</sub> crystalline phases) 7% selectivity to gluconic acid after 42% glucose conversion was achieved.

Aerobic and anaerobic photoconversion of glucose were studied by Bellardita et al. [99] by using Pt-TiO<sub>2</sub> anatase, rutile and brookite samples in aqueous media. Under anaerobic conditions H<sub>2</sub> was obtained only in the presence of Pt. Under both aerated and anaerobic conditions, the photoisomerization to fructose and the oxidation to products as gluconic acid, arabinose, erythrose and formic acid, was observed, whereas under anaerobic condition, together with the same partial oxidation products also a significant amount of H<sub>2</sub> was produced. The presence of Pt increased the mineralization rate of glucose without changing the type of products. The good H<sub>2</sub> evolution can be explained by taking into account the high value of Pt working function. A different distribution of the intermediates was observed: gluconic acid was prevalently obtained with anatase while rutile and brookite gave preferential rise to arabinose and erythrose. Rutile and brookite were more active than anatase both towards glucose conversion and H<sub>2</sub> production obtaining ca.1700 mmol of H<sub>2</sub> after 7 h of irradiation.

Visible-light responsive bare and metal loaded TiO<sub>2</sub> photocatalysts were obtained by using a simple ultrasonic method [102]. This method induced bulk oxygen deficiency resulting in a decrease of band gap. Pt-P25 treated at 40 kHz for 2 h showed higher conversion of glucose and higher H<sub>2</sub> production under solar irradiation with respect to the untreated sample. This was due to the shift of the valence band edge responsible for the visible light absorption.

Doping with metallic and non-metallic species has been also explored to improve the TiO<sub>2</sub> efficiency and to better exploit the solar radiation. Bellardita et al. [103] prepared a series of W and N Pt-TiO<sub>2</sub> (rutile) doped samples with the aim to extend the absorption to the visible light and to enhance the separation between the photogenerated electrons and holes. The experiments were carried out under anaerobic conditions under simulated or natural sunlight irradiation. The presence of nitrogen did not influence the glucose conversion but increased the selectivity to arabinose and formic acid and decreased the H<sub>2</sub> production. On the other hand, W had a negative effect on glucose conversion but a beneficial effect on H<sub>2</sub> evolution.

Nwosu et al. [104] reported the synthesis of a titanium-based perovskite (NiTiO<sub>3</sub>) active under visible light and studied the effects of reaction conditions on the selectivity towards the intermediates obtained during the glucose photoreforming. AA carried out a systematic investigation of the relationship between different reaction parameters (substrate, concentrations, reaction times, solvent pH values, solvent compositions, and reaction atmospheres) and product selectivity obtaining 75% selectivity towards arabinose in neutral conditions and a total 63% selectivity towards lactic acid, acetic acid, and formic acid in alkaline conditions.



Bi<sub>2</sub>WO<sub>6</sub>/CoPz (cobalt tetra (2,3-bis(butylthio)maleonitrile) porphyrazine) composite was used for the selective photocatalytic oxidation of glucose to high value-added chemicals in aqueous media using atmospheric O<sub>2</sub> as the oxidant and solar light as the driving force [105]. The highest activity for Bi<sub>2</sub>WO<sub>6</sub>/CoPz composite was obtained with a CoPz content of 0.25%. The total selectivity towards arabinose and formic acid was 96.8% for 45.3% of glucose conversion that was achieved after 3h.

Nitrogen-deficient carbon nitride (BNCN) and chlorine 6 (Ce6) can efficiently and selectively oxidize glucose into gluconic and glucaric acid [106]. The resultant Ce6@BNCN composite catalyst gave a total selectivity towards gluconic acid, glucaric acid and arabinose as high as 70.9% at glucose conversion up to 62.3%, and the above figure is superior to previously reported photocatalytic systems.

The highly selective photocatalytic conversion of glucose solution on holo-symmetrically spherical three-dimensionally ordered macroporous TiO<sub>2</sub>-CdSe heterojunction photonic crystal structure (s-TCS) was reported by Wang et al. [107]. The photocatalysts showed excellent stability and efficient photogenerated electrons/holes separation. With a glucose conversion of about 95.9%, the selectivity towards lactic acid was 94.3%. For the first time, they revealed that the photocatalytic conversion of glucose to lactic acid is a third-order and four-electron-involved reaction.

BiOBr/Zn@SnO<sub>2</sub> (ratio 3:1) coupled photocatalyst showed good performance during fructose selective oxidation in aqueous alkaline solution under simulated solar light irradiation [108]. Fructose conversion was almost 100%, and the lactic acid yield was 79.6% under optimal reaction conditions. The catalyst proved to be stable and reusable because, even after five runs it was possible to obtain a lactic acid yield of 67.4%.

#### **2.2.4 5-Hydroxymethyl-2-furaldehyde (HMF)**

The HMF molecule, produced from monosaccharides with six carbon atoms, is a key precursor for the synthesis of chemicals in pharmaceutical and polymer industries [73,109,110]. Starting by HMF as substrates, different high value compounds can be formed by varying the photocatalyst and the experimental conditions. For example, 2,5-furan dicarboxylic acid (FDCA), one of the HMF oxidation products, can be used as a monomer to produce desired polymeric materials [111,112]. In Figure 5 is reported a scheme of the reaction pathway related to the partial oxidation of HMF to the possible derivatives.

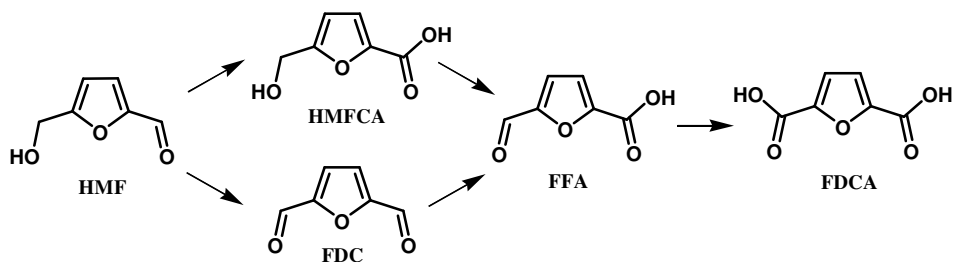


**Figure 5.** Proposed reaction pathway for 5-HMF partial oxidation [39].

Yurdakal and co-workers [113] first in 2013 applied the photocatalytic method to the selective oxidation of HMF in aqueous medium under UVA light irradiation in the presence of different commercial and laboratory made anatase, rutile, and brookite TiO<sub>2</sub> photocatalysts. The main products detected were FDC and CO<sub>2</sub> with all of the catalysts and the homemade samples showed higher activity than the commercial ones with a FDC selectivity of 22% for a HMF conversion of 50%. Similar results were found by using TiO<sub>2</sub> nanoparticles synthesized by an electrochemical method reaching 25% selectivity towards FDC [114]. Lolli et al. [109] during the selective photocatalytic oxidation of HMF with commercial (TiO<sub>2</sub>-c) and homemade (TiO<sub>2</sub>-m) TiO<sub>2</sub> catalysts using a solar simulator as irradiation source, found HMFCFA as the main intermediate when Na<sub>2</sub>CO<sub>3</sub> was present in the aqueous solution. The selectivity reached 25% with a conversion of 22% by using the TiO<sub>2</sub>-m sample. In the presence of the commercial sample, a higher conversion and a lower selectivity was observed. The main active species implied in the HMF oxidation are the O<sub>2</sub><sup>·-</sup> radicals.

Ag nanoparticles supported on TiO<sub>2</sub> (2.5%Ag/TiO<sub>2</sub>) displayed high activity towards partial oxidation of HMF in aqueous solution containing Na<sub>2</sub>CO<sub>3</sub> raising the selectivity towards HMFCFA up to ca. 97% under visible-light irradiation [115]. The excellent performance has been attributed to the enhanced localized surface plasmon resonance (LSPR) effects deriving from the presence of Ag nanoparticles of appropriate size.

TiO<sub>2</sub> based photocatalysts generally displayed low selectivity values towards the different intermediates deriving from HMF due to the formation of highly reactive HO<sup>·</sup> radicals under irradiation which attack nonselectively organic substrates. To this end, alternative photocatalysts have been studied, and among these a good candidate is C<sub>3</sub>N<sub>4</sub> due to the moderate oxidation ability of the holes generated in its conduction band [110,116,117].

Wu et al. [118] found that the graphitic C<sub>3</sub>N<sub>4</sub> samples prepared starting from melamine by simple calcination gives rise to partial oxidation of HMF to FDC with a selectivity of only 21.1% at a HMF conversion of 29.9% under simulated solar light irradiation and O<sub>2</sub> flow.

Graphitic  $C_3N_4$  obtained by melamine via a thermal condensation method showed good photocatalytic activity for the partial oxidation of HMF in water to FDC under both artificial UV and real solar irradiation, with a maximum selectivities of ca. 45% at a HMF conversion of ca. 50% under natural solar light irradiation [119]. Runs carried out in a pilot plant photoreactor irradiated by solar light by using an adduct  $C_3N_4-H_2O_2$  as photocatalyst showed the same results obtained in the laboratory scale reactor [120]. The efficiency depended also on the precursor used for the synthesis of  $C_3N_4$  and on the thermal treatment to which it was subjected.

Cobalt thioporphyrine coupled with graphitic carbon nitride  $g-C_3N_4$  (CoPz/ $g-C_3N_4$ ) displayed high activity towards the selective conversion of HMF to 2,5-furandicarboxylic acid (FDCA) under green conditions (simulated sunlight, ambient conditions, atmospheric air as  $O_2$  source), in aqueous medium in the presence at different pH values [121]. The formed products depended on the solution pH, and a good amount of FDC was preferentially formed under slightly acidic conditions, whilst FDCA was the main product under the acidic ones with a yield of 96.1%.

Also  $g-C_3N_4$  and  $NaNbO_3$  ( $g-C_3N_4/NaNbO_3$ ) formed an efficient heterojunction displaying higher activity than pure  $g-C_3N_4$  in the partial oxidation of HMF to FFCA under  $O_2$  flow and irradiation by a 300 W xenon lamp [122]. A maximum HMF conversion of 35.8% along with a selectivity to FFCA of 87.4% was attained.

In recent years, in addition to  $C_3N_4$ , several alternative catalysts to  $TiO_2$  have been used for the valorization of HMF in aqueous medium and preferably using sunlight as the irradiation source. Ye et al. [123] used for the first time P-doped  $Zn_xCd_{1-x}S$  solid solutions as the photocatalysts for the contemporary HMF oxidation and  $H_2$  evolution. They irradiated the set-up with a white LED as the irradiation source. A good  $H_2$  production along with the formation of FDC was obtained.

$MoS_2/CdIn_2S_4$  heterojunctions revealed high activity for selective oxidation of HMF into FDC in aqueous solution under visible-light irradiation [124]. Transient photocurrent response, EIS Nyquist plots and PL spectra demonstrated an enhanced separation of photogenerated charges with respect to bare  $CdIn_2S_4$  due to the formation of a heterojunction between the two components (Figure 5). The presence of  $MoS_2$  promotes the charges separation, while its amount influenced the photocatalytic activity. In the presence of the composite containing 12.5% of  $MoS_2$ , under the optimized conditions, 80.93% of FDC selectivity was achieved along with a HMF conversion of 61.73%. Mechanistic studies suggested that  $O_2^{\cdot-}$  radicals are the main active species for HMF oxidation.

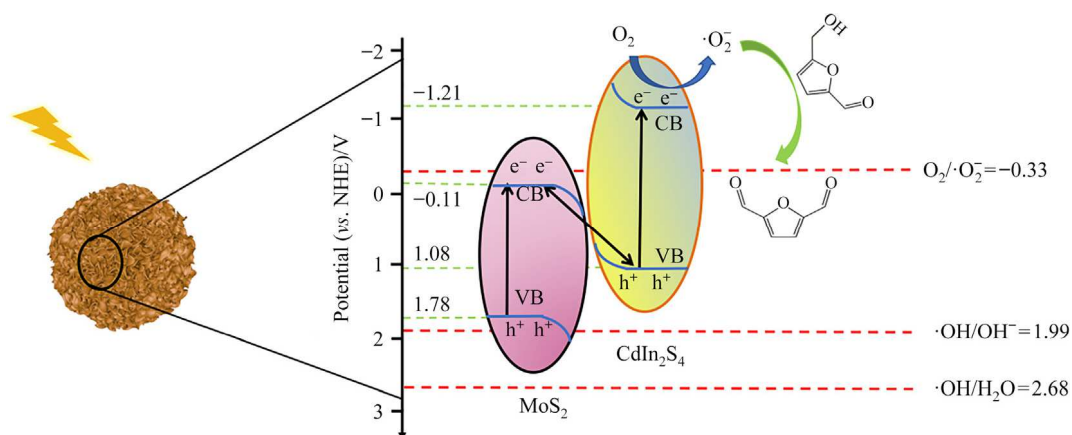


**Figure 6.** HMF oxidation on MoS<sub>2</sub>/CdIn<sub>2</sub>S<sub>4</sub> heterojunctions [124].

Dhingra et al. [125] coupled the selective oxidation of HMF to FDC with H<sub>2</sub> production by using Zn<sub>0.5</sub>Cd<sub>0.5</sub>S/xMnO<sub>2</sub> under visible light irradiation. A FDC yield of 46% and 14% with a contemporary H<sub>2</sub> production of 1322 μmol g<sup>-1</sup> and 152.6 μmol g<sup>-1</sup> in 24 h were obtained under simulated and natural solar light irradiation, respectively.

### 2.2.5 3-Pyridine-methanol

The commercially valuable product deriving from 3-pyridinemethanol is vitamin B<sub>3</sub> (nicotinic acid), which is considered as one of the 80 essential human nutrients and is generally used to prevent pellagra disease and alcoholism.

Alfè et al. [126] applied the photocatalytic method by using TiO<sub>2</sub>/graphene-like composite photocatalysts to the selective oxidation of 3-pyridine-methanol under both UV and simulated solar light irradiation in aqueous solution containing cupric ions. 3-Pyridine carboxyaldehyde and vitamin B<sub>3</sub> were the identified products. Under the optimized conditions an alcohol conversion degree of 63.3% was reached with a yield of 39.5% for 3-pyridine carboxyaldehyde and 22% for vitamin B<sub>3</sub> [127]. Low crystalline laboratory made rutile TiO<sub>2</sub> was more efficient than commercial samples under both UV and visible light irradiation. The highest selectivity towards vitamin B<sub>3</sub> was 75% when the alcohol conversion was 50% at pH 12 under UV irradiation.

## 3. Photoelectrocatalytic partial oxidation reactions

This section summarizes the synthesis of commercially valuable products by the photoelectrocatalytic method in water solvent. The first PEC reaction was investigated by

Bettoni et al. in 2011 [128]; however, only in the last few years has scientists' interest in studies in this field increased. Consequently, the articles on photocatalytic synthesis research are higher than those on PEC. Even if the PEC synthesis reactions are generally performed in organic solvents such as acetonitrile, all syntheses reported in this review were performed in water due to their potential importance from an environmental point of view. In addition, the presented PEC reactions were performed at room temperature and ambient pressure under UVA, UVA-Vis, Vis, and/or solar light. Consequently, the experimental conditions are environmentally friendly. However, some PEC works have been performed at high electrolyte concentrations (up to 500 mM), at very acidic pH's, and using soluble mediators/co-catalysts to increase yields. The latter works could not be considered green, and often involve additional costs and problems in separating the product(s).

Moreover, although simultaneous production of H<sub>2</sub> also can occur during the PEC syntheses, in some cases this important reaction is ignored, at least in the title of the paper.

### 3.1 Benzyl alcohols

P-anisaldehyde (PAA), the main oxidation product of 4-methoxybenzyl alcohol, is widely used in the fragrance and flavour industry. Moreover, it is used in the synthesis of some molecules in pharmaceuticals and perfumery [129]. Bettoni et al. performed selective photoelectrocatalytic oxidation of 4-methoxybenzyl alcohol (4-MBA, initial concentration: 2.5 mM) to PAA under UV-Vis irradiation by using Ti/TiO<sub>2</sub> electrode in water. Ti/TiO<sub>2</sub> plate was prepared by thermal oxidation of a Ti plate at 700 °C in air [128]. A two-electrodes system was used in the PEC method in which the Ti plate is the cathode. Some experiments were also performed in acetonitrile instead of water for the sake of comparison. A lower current efficiency (18% vs. 88) and PAA yield (10% vs. 27%) with PEC experiments in water conducted for four hours were obtained compared to acetonitrile.

Özcan and et al. performed the selective oxidation of substituted benzyl alcohol in water under UV-Vis irradiation using a batch reactor with a three-electrode system [130]. The Ti/TiO<sub>2</sub> electrodes were prepared by thermal oxidation of the Ti plate (400-700 °C) or by dip-coating method using TiCl<sub>4</sub> as the precursor and following the calcination process (up to 850 °C). The thin films of TiO<sub>2</sub> on the electrodes can be used without their morphology being modified with loss of activity as they are resistant to breakage and photocorrosion.

The calcined electrodes showed slightly better activity and selectivity to the product(s) than the dip-coated ones. Table 3 summarizes the PEC results of benzyl alcohol (BA) derivatives using

a one-layer dip coated TiO<sub>2</sub> layer and thermally oxidized TiO<sub>2</sub> plates, with the oxide mostly in the rutile phase.

The results obtained show that in the presence of an electron donor group in the para and/or ortho position of BA, the conversion rate and selectivity to the corresponding aldehyde increased. The electron donor group, in fact, increases the density of the electronic cloud of the aromatic ring and this contributes to increasing the oxidation rate [48,130]. The highest activity and selectivity values were obtained with 4-MBA oxidation, while 4-nitrobenzyl alcohol (4-NBA) showed the worst ones. In fact, the selectivity towards 4-nitrobenzaldehyde was only 2-3% with both types of electrodes. Notably, these PEC results coincide with those obtained by performing the same reactions under photocatalytic conditions using powdered TiO<sub>2</sub> catalysts [48].

**Table 3.** The PEC oxidation results of substituted aromatic alcohols (0.5 mM) using a one-layer dip coated and following calcination at 700 °C (Ti/TiO<sub>2</sub>-Dip-Coated-700) and thermally oxidized at 500 °C (Ti/TiO<sub>2</sub>-Therm.Ox-500) plates in water under UV-Vis irradiation. Applied potential: 0.75 V [130].

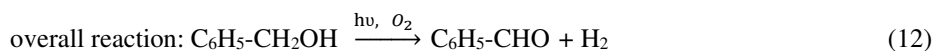
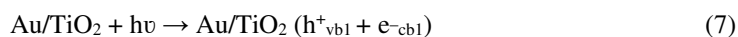
Catalyst	<sup>a</sup> Substrate	<sup>b</sup> r <sub>0</sub> (μM·h <sup>-1</sup> )	<sup>c</sup> Selectivity (%)
Ti/TiO <sub>2</sub> -Dip-Coated-700	4-MBA	134	90
Ti/TiO <sub>2</sub> -Therm.Ox-500	4-MBA	151	85
Ti/TiO <sub>2</sub> -Dip-Coated-700	BA	32.4	13
Ti/TiO <sub>2</sub> -Therm.Ox-500	BA	24.9	20
Ti/TiO <sub>2</sub> -Dip-Coated-700	2-MBA	130	60
Ti/TiO <sub>2</sub> -Therm.Ox-500	2-MBA	164	70
Ti/TiO <sub>2</sub> -Dip-Coated-700	3-MBA	46.9	9
Ti/TiO <sub>2</sub> -Therm.Ox-500	3-MBA	40.8	16
Ti/TiO <sub>2</sub> -Dip-Coated-700	2,4-DMBA	288	54
Ti/TiO <sub>2</sub> -Therm.Ox-500	2,4-DMBA	288	50
Ti/TiO <sub>2</sub> -Dip-Coated-700	2,3,4-TMBA	104	35
Ti/TiO <sub>2</sub> -Therm.Ox-500	2,3,4-TMBA	102	37
Ti/TiO <sub>2</sub> -Dip-Coated-700	4-NBA	32.9	3
Ti/TiO <sub>2</sub> -Therm.Ox-500	4-NBA	46.9	2
Ti/TiO <sub>2</sub> -Dip-Coated-700	4-HBA	43.5	11

Catalyst	<sup>a</sup> Substrate	<sup>b</sup> $r_0$ ( $\mu\text{M}\cdot\text{h}^{-1}$ )	<sup>c</sup> Selectivity (%)
Ti/TiO <sub>2</sub> -Therm.Ox-500	4-HBA	31.4	12

<sup>a</sup>BA: Benzyl alcohol; 2-MBA: 2-methoxybenzyl alcohol; 3-MBA: 3-methoxybenzyl alcohol; 2,4-DMBA: 2,4-dimethoxybenzyl alcohol; 2,3,4-TMBA: 2,3,4-trimethoxybenzyl alcohol; 4-NBA: 4-nitrobenzyl alcohol; 4-HBA: 4-hydroxybenzyl alcohol. <sup>b</sup>Initial reaction rate,  $r_0$ . <sup>c</sup>Selectivity to the corresponding aldehydes was determined after 25% alcohol conversion.

The simultaneous PEC oxidation of benzyl alcohol and H<sub>2</sub> generation was also studied by Wu et al. using an in situ doped Au/TiO<sub>2</sub> nanotube anode under simulated solar light in water [131]. The Au/TiO<sub>2</sub> nanotube was prepared by an anodic oxidation method in an ethylene glycol medium (in the presence of 0.2 M HF and 1 M H<sub>2</sub>O), starting from an Au/Ti alloy plate (0.2% Au). Carbon-doped Cu<sub>2</sub>O nanowires on Cu mesh (C/Cu<sub>2</sub>O/Cu) were used as the cathode. The PEC experiment results obtained using different photoanode/photocathode systems are reported in Table 4. Notably, (Au/TiO<sub>2</sub>)/(C/Cu<sub>2</sub>O/Cu) anode/cathode system in aerobic condition showed much more substrate activity (conversion: 85%) with respect to the conditions in which undoped TiO<sub>2</sub> nanotube was used as the anode ((TiO<sub>2</sub>)/(C/Cu<sub>2</sub>O/Cu) conversion: 55%) or Pt as the cathode ((Au/TiO<sub>2</sub>)/(Pt) conversion: 48%).

The highest H<sub>2</sub> production amount and efficiency were achieved by using the (Au/TiO<sub>2</sub>)/(C/Cu<sub>2</sub>O/Cu) system, due to the tuning effect of Au, which reduced electron-hole recombination. In aerobic conditions the selectivity values towards benzaldehyde are very high (99%), while in anaerobic conditions both a modest selectivity towards benzaldehyde (50%) and a low conversion of benzyl alcohol were obtained. The high selectivity under aerobic conditions could be due to the production of superoxide radicals instead of hydroxyl radicals, usually considered non-selective oxidizing species. The proposed reaction mechanism for the production of benzaldehyde and H<sub>2</sub> under aerobic conditions is summarized in Eqs 7-12. Eqs 7-8 occur at the photoanode, while Eqs 9-11 at the photocathode.



Electron and hole pairs on the anode (Au/TiO<sub>2</sub>) surface are generated by solar light, and the adsorbed benzyl alcohol molecules on the anode are oxidized by h<sup>+</sup> to the benzyl alcohol active cation (\*C<sub>6</sub>H<sub>5</sub>-CH<sub>2</sub>OH<sup>+</sup>), while oxygen molecules reduce to the superoxide radicals O<sub>2</sub><sup>·-</sup> (see the scheme in Figure 7). After that, the combination of \*C<sub>6</sub>H<sub>5</sub>-CH<sub>2</sub>OH<sup>+</sup> and O<sub>2</sub><sup>·-</sup> produces benzaldehyde, H<sup>+</sup>, and O<sub>2</sub>. In the oxygenated medium, O<sub>2</sub> is first reduced by generated electrons, and the obtained O<sub>2</sub><sup>·-</sup> preferentially combines with the \*C<sub>6</sub>H<sub>5</sub>-CH<sub>2</sub>OH<sup>+</sup>. Consequently, the benzyl alcohol can be oxidized to benzaldehyde with high selectivity. In this system O<sub>2</sub> acts as a catalyst.

The structure of this dual electrode photoelectrochemical cell is an isolated Z-scheme (Figure 7). The produced H<sup>+</sup> by the BA oxidation reaction on the anode transfers through the PEM (perfluorinated cation exchange membrane) to the cathode area and is reduced by e<sup>-</sup> to produce H<sub>2</sub>. Meanwhile, the generated electrons on the anode are transferred through the metal wire and combined with the generated holes at the cathode, which further improves the efficiency of anodic oxidation and cathodic H<sub>2</sub> production reactions. The anodic oxidation reaction of the whole system is the rate-determining step; consequently, the H<sub>2</sub> production efficiency depends on the anodic oxidation reaction.

**Table 4.** Selective PEC results of simultaneous oxidation of benzyl alcohol and H<sub>2</sub> generation by different anode/cathode systems under simulated solar light in water [131].

Electrode system	Substrate	Condition	Conversion (%)	S <sub>BAD</sub>	J <sub>o</sub> (mA·cm <sup>-2</sup> )	H <sub>2,exper</sub> <sup>a</sup>	H <sub>2</sub> efficiency (%)
(Au/TiO <sub>2</sub> )/(Cu <sub>2</sub> O)	BA	Aerobic	85	99	0.5	143.83	84.6
(TiO <sub>2</sub> )/(Cu <sub>2</sub> O)	BA	Aerobic	55	99	0.46	90.05	81.8
(Au/TiO <sub>2</sub> )/(Cu <sub>2</sub> O)	BA	Anaerobic	61	50	0.4	79.25	<65.0
(Au/TiO <sub>2</sub> )-(Pt)	BA	Aerobic	48	99	0.065	47.04	49.0
(Au/TiO <sub>2</sub> )-(Cu <sub>2</sub> O)	blank	Aerobic			0.045	10.42	

<sup>a</sup>H<sub>2,exper</sub> represents the experimental H<sub>2</sub> production amount. Initial benzyl alcohol concentration: 100 μM.

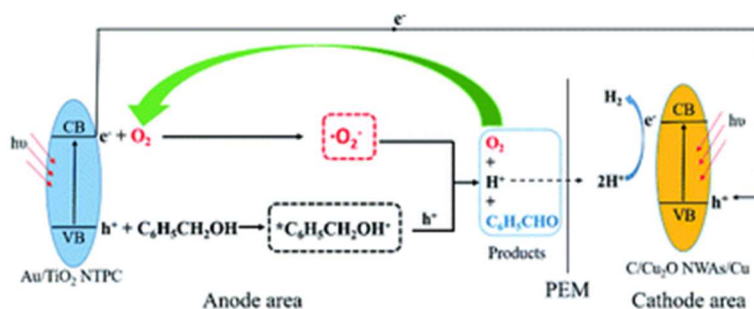




**Figure 7** The Proposed PEC reaction mechanism for the benzyl alcohol oxidation and H<sub>2</sub> production in a dual electrode photoelectrochemical cell in aerobic condition under simulated solar irradiation (AM 1.5) [131].

Hydrogen is a promising alternative energy source and could also be produced from PEC water splitting reaction under solar irradiation. The oxygen evolution reaction (OER), the rate-determining step, involves four electrons, while the hydrogen evolution reaction (HER) involves two electrons. Therefore, H<sub>2</sub> production efficiency increases by decreasing the overpotential of OER. In order to increase HER efficiency, thermodynamically more favourable reactions (e.g., oxidation of biomass derivatives) could replace OER [132,133].

Simultaneous selective PEC benzyl alcohol oxidation and H<sub>2</sub> production in water and under solar light were investigated by Zhou and co-workers [134]. Bi<sub>2</sub>MoO<sub>6</sub> loaded nanotube structured TiO<sub>2</sub> was used as the photoanode, while carbon-doped nanowire structured Cu<sub>2</sub>O was the photocathode (see Figure 8). Table 5 shows experimental results of simultaneous PEC BA oxidation and H<sub>2</sub> production. Bi<sub>2</sub>MoO<sub>6</sub>@TiO<sub>2</sub>-C/Cu<sub>2</sub>O (anode-cathode) system showed the best BA conversion (67%) and selectivity towards benzaldehyde (99%) results in an oxygen atmosphere. In this photoanode-photocathode system, more H<sub>2</sub> (5.5 fold) was produced with respect to that obtained when OER was used (115 vs. 20 μmol·cm<sup>-2</sup>). In the presence of O<sub>2</sub>, better results of selectivity towards BAD were obtained due to the production of O<sub>2</sub><sup>•-</sup> radicals, similar to the work of Wu et al. [131]. In addition, the photoanode kind could change the reaction mechanism; hydroxyl radicals were formed on the TiO<sub>2</sub> anode (even in O<sub>2</sub> atmosphere), while they were not involved on a Bi<sub>2</sub>MoO<sub>6</sub>@TiO<sub>2</sub> surface at the photoanode position, according to the EPR analysis. Because of strongly oxidizing hydroxyl radicals, a low value of selectivity towards BAD (58%, Table 5) was obtained in the presence of TiO<sub>2</sub> as a photoanode (TiO<sub>2</sub>-C/Cu<sub>2</sub>O system).

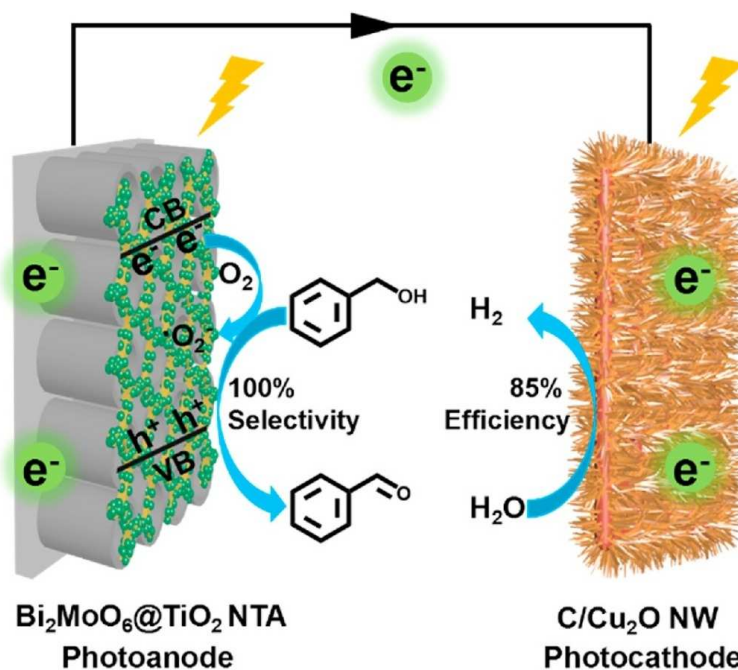


**Figure 8** Illustration of a PEC cell where both cathodic and anodic reactions occur simultaneously. NTA: nanotube array; NW: nanowire [134].

**Table 5.** PEC simultaneous benzyl alcohol oxidation and H<sub>2</sub> production in water and under solar irradiation under aerobic/anaerobic conditions [134].

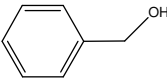
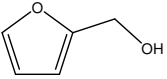
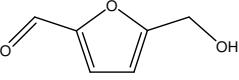
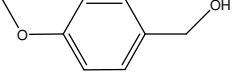
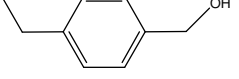
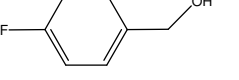
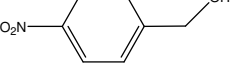
Photoanode/photocathode	Condition	$J_0$ (mA·cm <sup>-2</sup> )	Conversion (%)	Selectivity towards BAD (%)	H <sub>2</sub> (μM cm <sup>-2</sup> )	H <sub>2</sub> efficiency (%)
Bi <sub>2</sub> MoO <sub>6</sub> @TiO <sub>2</sub> -C/Cu <sub>2</sub> O	anaerobic	0.32	48	46	60	62
TiO <sub>2</sub> -C/Cu <sub>2</sub> O	anaerobic	0.33	51	37	52	59
Bi <sub>2</sub> MoO <sub>6</sub> @TiO <sub>2</sub> /Pt	aerobic	0.24	43	98	34	40
Bi <sub>2</sub> MoO <sub>6</sub> @TiO <sub>2</sub> -C/Cu <sub>2</sub> O	aerobic	0.54	67	99	115	85
TiO <sub>2</sub> -C/Cu <sub>2</sub> O	aerobic	0.36	69	58	92	67
Bi <sub>2</sub> MoO <sub>6</sub> @TiO <sub>2</sub> -C/Cu <sub>2</sub> O*	aerobic	0.09	–	–	21	–

\*Experiment performed without BA. PEC reaction time: 8 h. Initial benzyl alcohol concentration: 100 mM dissolved in 100 mM Na<sub>2</sub>SO<sub>4</sub> aqueous solution.

Table 6 shows experimental results of selective PEC oxidation of furan and para-substituted benzyl alcohol derivatives by Bi<sub>2</sub>MoO<sub>6</sub>@TiO<sub>2</sub>-C/Cu<sub>2</sub>O system under aerobic conditions [134]. Selectivity towards 2,5-furandicarbaldehyde (FDC) and produced H<sub>2</sub> amount were only 47% and 32 μM·cm<sup>-2</sup>, respectively. On the contrary, selectivity to other corresponding aldehydes

and produced H<sub>2</sub> from other substrates oxidation were very high, ca. 99% and ca. 110 μM·cm<sup>-2</sup>, respectively. Moreover, benzyl alcohols with electron donor groups at para position (e.g., -OCH<sub>3</sub>, -CH<sub>3</sub>) showed better selectivity values towards aldehyde and H<sub>2</sub> production yield than those bearing electron-withdrawing groups (e.g., -F, -NO<sub>2</sub>), as expected [130].

**Table 6.** Experimental results of selective PEC oxidation of furan and different *p*-substituted benzyl alcohol derivatives by Bi<sub>2</sub>MoO<sub>6</sub>@TiO<sub>2</sub>-C/Cu<sub>2</sub>O system under aerobic condition [134].

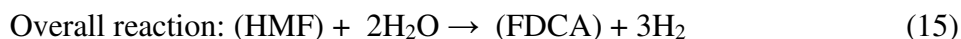
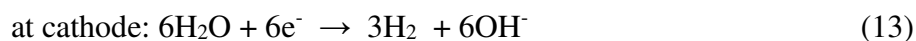
Substrate	Conversion (%)	Selectivity to aldehyde (%)	<i>J</i> <sub>0</sub> (mA·cm <sup>-2</sup> )	H <sub>2</sub> (μM·cm <sup>-2</sup> )	H <sub>2</sub> efficiency (%)
	67	99	0.54	115	85
	63	98	0.53	104	84
	55	47	0.50	32	61
	72	99	0.56	125	87
	69	98	0.54	119	86
	65	98	0.53	109	84
	62	98	0.52	103	83
<b>Water</b>	–	–	0.09	21	–

Pulignani et al. [135] investigated high-performance carbon nitride-based electrode for selective PEC oxidation of 4-methylbenzyl alcohol to 4-methylbenzaldehyde (*p*-tolualdehyde) in water at pH 7 in Na<sub>2</sub>SO<sub>4</sub> solution (0.1 M) in a single compartment under simulated solar light. In the photoanode, cyanamide-functionalized carbon nitride was co-deposited with ITO nanoparticles on a 1.8 Å thick Al<sub>2</sub>O<sub>3</sub>-coated FTO electrode. In the investigated material, ITO nanoparticles act as a conductive binder and improve electron extraction from the cyanamide-

functionalized carbon nitride, while the alumina underlayer reduces recombination losses between the ITO and the FTO glass. Initial 4-methylbenzyl alcohol concentration was not low (50 mM); consequently, only 22.3 % substrate conversion after 18h of the PEC reaction was observed.

### 3.2 HMF

Partial electrochemical and PEC oxidations of HMF in water and under solar irradiation in the presence of 2,2,6,6-tetramethylpiperidine 1-oxyl radical (TEMPO) as a mediator and BiVO<sub>4</sub> as a photoanode were investigated by Cha and Choi [136]. The reaction mechanism for 5-formyl-2-furoic acid (FFA) and FDCA formations is through 5-hydroxymethyl-2-furancarboxylic acid (HMFCFA), while in the presence of TEMPO it is through 2,5-diformylfuran (FDC) (Figure 9). Table 7 reports the (photo)electrochemical conversion values of HMF and products yield versus the circulated electric charge. At 40 Coulomb, complete HMF conversion (100%) and high FDCA selectivity (ca. 99%) both for EC and PEC were obtained. The proposed reaction mechanism is reported below (Eq. 13-15). The photogenerated electrons were transferred to the Pt counter electrode to produce H<sub>2</sub> from water, while the holes on BiVO<sub>4</sub> were used for the HMF oxidation mediated by TEMPO (See Figure 9).



The experimental results of PEC and EC are similar; however, 0.5 V lower potential was used for PEC with respect to EC ones thanks to e<sup>-</sup>/h<sup>+</sup> generation on the BiVO<sub>4</sub> by solar light. Schematic illustrations of the (photo)electrochemical TEMPO-mediated HMF oxidation are shown in Figure 9. The photogenerated holes at the valance band of the BiVO<sub>4</sub> could be used both for HMF and water oxidation [136]. However, photoelectrochemically TEMPO-mediated HMF oxidation at the BiVO<sub>4</sub> surface is more favourable both kinetically and thermodynamically than H<sub>2</sub>O oxidation since TEMPO oxidation was kinetically much faster than water. Consequently, a high FDCA yield was obtained in the presence of TEMPO and HMF.

**Table 7.** The electrochemical and photoelectrochemical HMF conversion and product yield values versus circulated electric charge [42].

Method	Electric charge circulated (C)	HMF conversion (%)	FFA yield (%)	FDCA yield (%)	FDC yield (%)	HMFCFA yield (%)
EC	0	0	0	0	0	0
	10	63	52	5	7	< 1
	20	94	84	8	2	< 1
	30	99	26	73	trace	trace
	38	100	1	99	trace	trace
	40	100	trace	100	trace	trace
PEC	0	0	0	0	0	0
	10	59	52	1	7	trace
	20	89	78	7	3	< 1
	30	98	48	51	trace	trace
	38	99	16	82	trace	trace
	40	100	trace	98	trace	trace

Bias: 1.54 V (for EC) and 1.04 V (for PEC) were applied versus reversible hydrogen electrode (RHE) in 0.5 M borate buffer solution containing 5 mM HMF and 7.5 mM TEMPO. PEC runs were performed under AM 1.5 G illumination (100 mW). FFA: 5-formyl-2-furoic acid, FDCA: 2,5-furan-dicarboxylic acid, FDC: 2,5-diformylfuran, HMFCFA: 5-hydroxymethyl-2-furan-carboxylic acid.

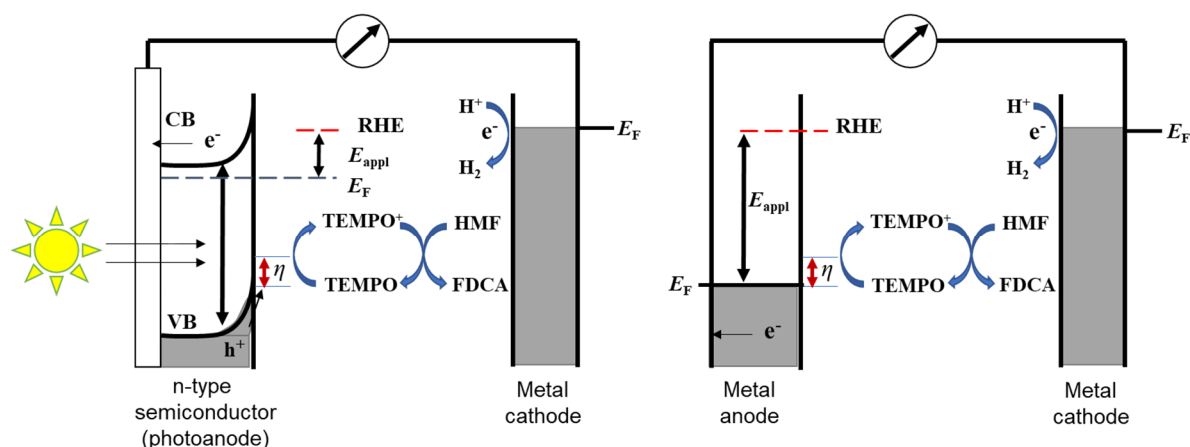


**Figure 9** Schematic illustration of photoelectrochemical TEMPO-mediated HMF oxidation (a) and electrochemical TEMPO-mediated HMF oxidation (b). CB, conduction band;  $E_F$ , Fermi energy [42].

Özcan and co-workers prepared nanotube-structured  $TiO_2$  on Ti layers (NT-Ti/ $TiO_2$ ), as photoanode, by anodic oxidation method in an ethylene glycol medium for PEC oxidation of HMF to FDC in water under UVA irradiation [137]. The NT-Ti/ $TiO_2$  plates were calcined at 400-750 °C, and they showed much better performance with respect to thin  $TiO_2$  layers on Ti plates prepared only by thermal oxidation (See Table 3). The NT-Ti/ $TiO_2$  samples were also platinized by the photoreduction method. The optimum calcination temperature was determined as 500 °C, and optimum bias and pH values for PEC experiments were found as 0.5 V and 5,

respectively. Interestingly, another intermediate, FFA, was also produced only in the presence of platinum catalyst. The Pt nanoparticles on the TiO<sub>2</sub> surface hinder the recombination of generated electron/hole pairs due to their electron trap role. Consequently, they allowed also higher performance (reaction rate and product selectivity) with respect to the pristine electrode: selectivity up to 40% towards FDC and 18% towards FFA after 10% conversion.

Figure 10 shows a representative run carried out by Pt-loaded nanotube structured photoanode versus time [137]. During the PEC reaction, HMF concentrations decrease while product concentrations increase. This increase, however, is not so significant due to the further oxidation reactions of the latter, so the selectivity values continuously decrease. For instance, selectivity value to FDC was 34% for 10% conversion, whereas it was only 19% for 60% conversion.

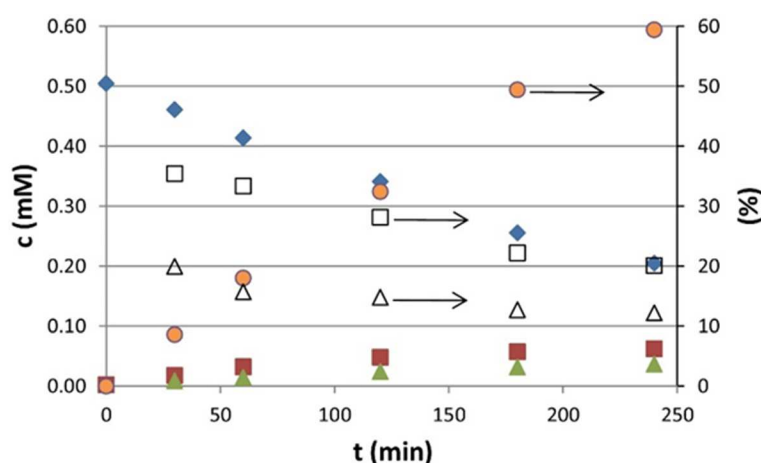


**Figure 10** Representative run of PEC oxidation of HMF vs. time using Pt-loaded nanotube structured photoanode at 0.50 V and pH 5 in water under UVA light. Concentrations of HMF (◆), FDC (■), and FFA (▲) are at the left axis; Selectivity towards FDC (□) and FFA (Δ) along with conversion (●) values are at the right axis [137].

2,5-Furandicarboxylic acid (FDCA), one of the main oxidation products of HMF, is a monomer for bioplastic production such as polyurethane, polyamide, and polyester [138,139]. Traditionally, synthesis conditions are not environmentally friendly, as they use noble metal catalysts, toxic oxidants, and high pressure and temperature, requiring high energy expenditure [140]. Pahari and Chen [141] investigated a catalyst composed of bismuth ferrite (BFO) nanosheets and few-layer phosphorene (FLP) with its surface modified with phosphate groups (P) to perform simultaneous H<sub>2</sub> production and selective HMF conversion to FDCA in water under neutral conditions and solar light. In the FLP-P-BFO-assisted OER of this study, the Fe centers of BFO offer the iron-oxo intermediate formation (Fe=O and Fe-OOH, determined by in situ Raman spectroscopy), and the phosphate groups modified on FLP help to stabilize the

Fe-OOH complex via a proton transfer. In 80 minutes, HMF (10 mM) totally transformed into FDCA with 100% selectivity and yield in the presence of 0.5 M Na<sub>2</sub>SO<sub>4</sub>.

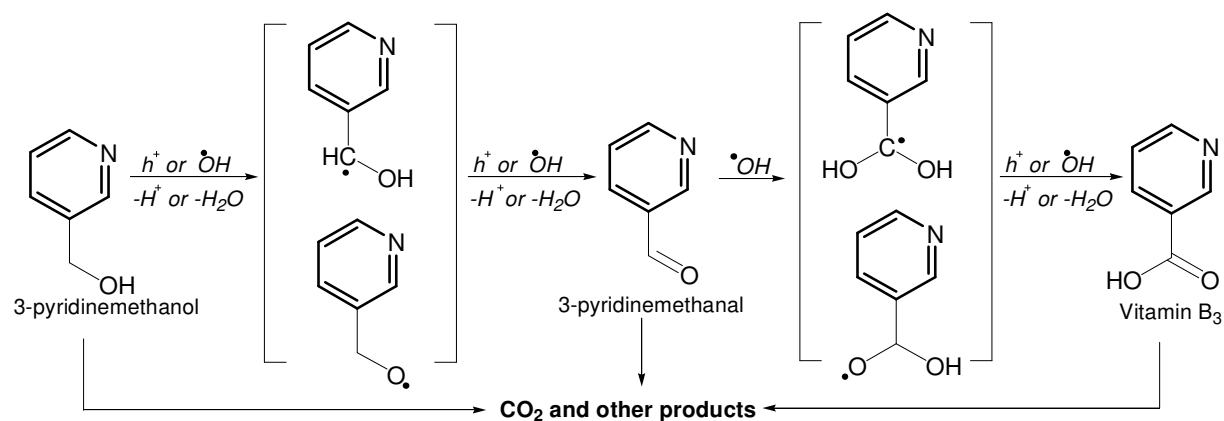
Chadderdon et al. [142] investigated cobalt phosphate (CoPi) loaded BiVO<sub>4</sub> photoanode for partial HMF oxidation mediated by TEMPO in water and under solar irradiation. TEMPO oxidation potential was reduced to 0.5 V by the presence of CoPi layer compared to that of pristine BiVO<sub>4</sub>. Notably, 88% selectivity to FDCA from PEC HMF oxidation was obtained with BiVO<sub>4</sub>/CoPi double-layer photoanode, whereas almost no FDCA formation was obtained with pristine BiVO<sub>4</sub>. Table 8 reports some experimental results of HMF oxidation and its product distribution versus transferred charge. The results show that the product FFA transforms into FDCA by increasing the transferred charge (time).

**Table 8.** Experimental results of PEC HMF oxidation and its product distribution versus transferred charge using cobalt phosphate loaded BiVO<sub>4</sub> photoanode. Applied potential: 0.64 V (versus RHE) under AM1.5 illumination in an electrolyte containing 5.0 mM TEMPO [142].

Transferred Charge (C)	HMF conversion (%)	FFA yield (%)	FDCA yield (%)	FDC yield (%)
0	0	0	0	0
3	58	7	5	9
6	91	67	22	3
9	99	58	78	1
12	100	4	88	<1

### 3.3.3 3-Pyridinemethanol

Yurdakal et al. [143] investigated nanotube-structured TiO<sub>2</sub> on Ti plates for PEC oxidation of 3-pyridinemethanol to 3-pyridinemethanal and vitamin B<sub>3</sub> in water under UVA irradiation. In Scheme 2 the reaction mechanism is proposed: 3-pyridinemethanol was oxidized to 3-pyridinemethanal by h<sup>+</sup> or hydroxyl radicals, followed by its oxidation to vitamin B<sub>3</sub>. The selectivity of the products decreased versus reaction time due to overoxidation of the products to open broken species and CO<sub>2</sub>.



**Scheme 2.** Proposed reaction mechanism for PEC oxidation of 3-pyridinemethanol to carbonyl derivatives and  $CO_2$  [143].

Photocatalytic and PEC 3-pyridinemethanol oxidations were performed both in  $N_2$  and  $O_2$  atmospheres. As expected, no photocatalytic oxidation was observed in  $N_2$  atmosphere, unlike what observed in the PEC process. Furthermore, PEC reactions were faster in  $N_2$  atmosphere than in  $O_2$  atmosphere.

3-Pyridinemethanal was also used as a substrate; it could be reduced to 3-pyridinemethanol at the cathode in the PEC reaction, although its oxidation to vitamin B<sub>3</sub> proved to be much more favoured [143]. Therefore, a H-type reactor in which the anode and cathode are divided is beneficial for the PEC synthesis reactions. In addition, the product selectivity was increased by decreasing the concentration of  $Na_2SO_4$  (as electrolyte) and the applied potential, although the reaction rate decreased. The reaction rate increased by increasing the stirring rate, probably due to an improvement in the mass transfer of the substrate (3-pyridinemethanol) from the bulk of the solution towards the surface and inside the nanotubes. In addition, the selectivity for 3-pyridinemethanal production increased since increasing its desorption rate hindered to overoxidation. For instance, 3-pyridinemethanal selectivity for 50% 3-pyridinemethanol conversion was 18% at 200 rpm, while it was 32% at 600 rpm.

The pH effect on the PC and PEC 3-pyridinemethanol oxidations was also investigated. Interestingly, no PC activity was observed at low pH (i.e., 2), and PC activity increased linearly by increasing pH. In an acidic medium, the stability of the aromatic ring is high due to the protonation of the nitrogen atom in the substrate's pyridine ring. However, PEC 3-pyridinemethanol oxidation could be performed at all pH values. In addition, selectivity towards vitamin B<sub>3</sub> increased by increasing the pH for PC reactions, while the PEC process was not significantly affected by the pH (see Table 9). However, PEC selectivity towards 3-pyridinemethanal decreased by increasing the pH. The results show that pH is an essential



parameter for the activity and selectivity to products, and its effect is different for PC and PEC reactions.

**Table 9.** The experimental results of 3-pyridinemethanol (0.5 mM) oxidation under UVA using the nanotube structure TiO<sub>2</sub> on Ti plate for different pH values. [Na<sub>2</sub>SO<sub>4</sub>] = 5 mM. Stirring speed: 400 rpm. Applied potential for PEC runs: 0.5 V vs Ag/AgCl (3M KCl) [143].

pH		$-r_0 \cdot 10^3$ (mM·h <sup>-1</sup> )	$k \cdot 10^3$ (h <sup>-1</sup> )	$t_{1/2}$ (h)	<sup>a</sup> S <sub>3-Pyridinemethanal</sub> (%)		<sup>b</sup> S <sub>Vitamin B3</sub> (%)		<sup>c</sup> S <sub>[CO<sub>2</sub>/6 X<sub>3h</sub></sub> (%)	X <sub>1h</sub> (%)	X <sub>3h</sub> (%)	pH X <sub>3h</sub>
					X <sub>0.15</sub>	X <sub>0.50</sub>	X <sub>0.15</sub>	X <sub>0.50</sub>				
2.31	PC	3.78	7.80							0	2	2.10
4.03	PC	34.7	59.5	11.6	45		9			6	16	4.02
7	PC	93.8	198	3.55	56		19		8.6	19	44	6.83
10.4	PC	120	218	3.18	27	33	49	35	1.0	22	48	8.12
12.4	PC	140	286	2.42	25	23	55	59	16	25	58	
2.38	PEC	153	415	1.67	54	48	29	36	5.3	30	71	2.21
4.04	PEC	179	375	1.85	44	31	32	37	22	31	68	3.61
7	PEC	134	271	2.50	42	27	45	36	21	25	55	6.24
10.1	PEC	167	320	2.16	40	24	32	35	21	31	63	7.91
12.4	PEC	125	307	2.26	22	6	45	38	31	25	60	11.9
12.4	*PEC	185	414	1.67	13	7	61	52	23	32	71	11.9

\*For this run Na<sub>2</sub>SO<sub>4</sub> was not used.

-r<sub>0</sub>: initial reaction rate, k: first-order rate constant, and t<sub>1/2</sub>: half life time.

<sup>a</sup>S<sub>3-Pyridinemethanal</sub> and <sup>b</sup>S<sub>Vitamin B3</sub>: 3-pyridinemethanal and vitamin B<sub>3</sub> selectivity values after 15% (X<sub>0.15</sub>) and 50% (X<sub>0.50</sub>) conversion. X<sub>1h</sub> and X<sub>3h</sub>: the conversion values after 1h and 3h of reaction times, respectively.

<sup>c</sup>CO<sub>2</sub> selectivity values were considered after 3h of reaction time (X<sub>3h</sub>).

The above work shows that selective PEC oxidation of 3-pyridinemethanol could be performed in environmentally friendly conditions in water at low applied potential (0.5 V), low electrolyte concentration (5 mM Na<sub>2</sub>SO<sub>4</sub>), under significant stirring speeds (at least 400 rpm) at all pH values.

In the second part of the work of Yurdakal et al. [144], the effect on the oxidation of 3-pyridinemethanol of loading some nanotube-structured TiO<sub>2</sub> plates with one or two noble metals present at the same time (Au, Pt and Pd) was studied. A high amount of metal loading negatively affected the PEC reaction since the metal prevented the light from penetrating inside the nanotubes. Nevertheless, a small amount of some metal as Pd slightly increased the PEC activity and selectivity to products with respect to the pristine plate. For instance, the conversion of the Pd-loaded catalyst and pristine one after 3h was 56 and 49%, while the selectivity towards 3-pyridinemethanal and vitamin B<sub>3</sub> after 50% conversion was 52 and 58%, respectively.

Moreover, a high 3-pyridinemethanal amount was obtained in the PC reaction, while the PEC produced a high amount of vitamin B<sub>3</sub>. In other words, the activity and the product distribution strongly depended on the process used.

### 3.4 Glycerol

Liu and co-workers investigated a nanoporous BiVO<sub>4</sub> catalyst for selective glycerol oxidation in water under solar irradiation [145]. The PEC reaction was performed at very acidic conditions (pH=2), and 200 mmol DHA per m<sup>2</sup> was produced with 51% selectivity. Glyceraldehyde (GDA), glyceric acid, and formic acid were the other products.

Gu and co-workers [146] also performed PEC glycerol oxidation using WO<sub>3</sub>/TiO<sub>2</sub> heterostructures on porous carbon fibers as 3-D microflow channels. This electrode showed a high reaction rate and GDA and DHA yields because a nanojunction improved charge separation, and the microchannel made mass transfer easier. For instance, total GDA and DHA selectivity was 85%, and their production rate was 35.3 μmol cm<sup>-2</sup> h<sup>-1</sup> at 1.2 V vs. RHE. Relatively low glyceric acid, formic acid, and CO<sub>2</sub> were also obtained (carbon balance: 92-97%).

PEC cyclohexane oxidation to cyclohexanol and cyclohexanone was also performed in the same system (yield: 12.8 μmol cm<sup>-2</sup>·h<sup>-1</sup>) [146]. Notably, an efficient photocatalytic fuel cell exhibiting short-circuit current of 1.2 mA·cm<sup>-2</sup> and a high open-circuit bias of 0.9 V was coupled with this microfluidic photoanode. The presence of the nanojunction in this two-in-one photocatalytic fuel cell system made it possible to obtain not only high added value products but also electricity (Figure 11).

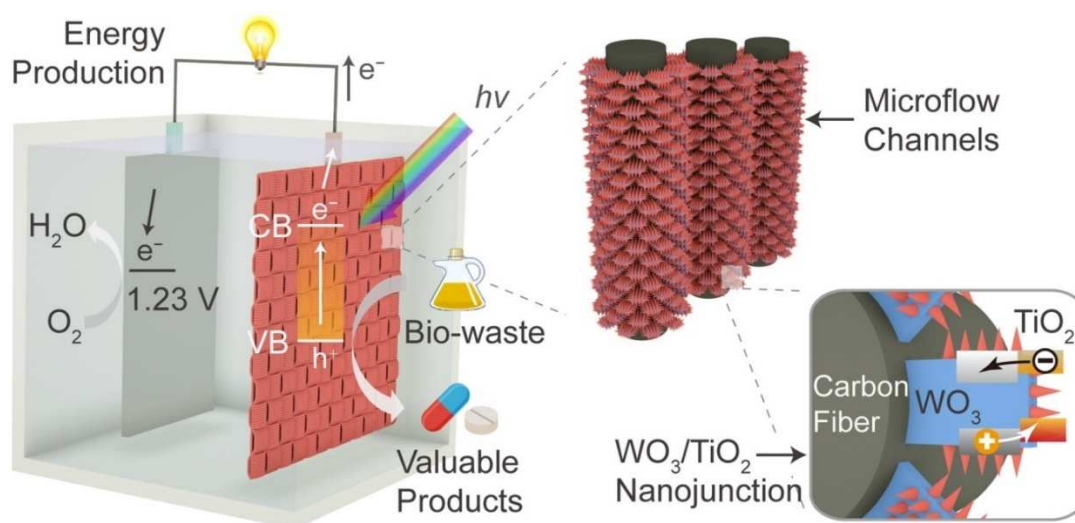


**Figure 11** Schematic illustration of photocatalytic fuel cell system for PEC biowaste oxidation on the WO<sub>3</sub>/TiO<sub>2</sub> heterostructures on porous carbon fibers as 3-D microflow channels [146].

Çetinkaya et al. [147] prepared nanotube, nanobelt, and nanosponge structured TiO<sub>2</sub> nanoparticles on Ti layers to perform PEC glycerol oxidation in water and under UVA irradiation. The optimum PEC performance was obtained in 20 mM Na<sub>2</sub>SO<sub>4</sub> at pH=7 and by applying 1.5 V. NaCl and KNO<sub>3</sub> as electrolytes were also tested, but Na<sub>2</sub>SO<sub>4</sub> showed to be the best one. In addition, the calcination temperature of the plates was determined as 500 °C. Thermally oxidized Ti/TiO<sub>2</sub> plate showed no activity for 4h of PEC reaction, while with nanotube and nanobelt structured samples, 35% conversion was obtained. In the PEC experiments, initial glycerol concentration was 10 mM. These results show that nanotube, nanosponge, and nanobelt structured samples have a much higher efficient surface area than the thin-film structured ones. However, product selectivity values of nanotube and nanobelt are low: 15% DHA, 6% GDA, and 15% formic acid. Moreover, ca. 20% CO<sub>2</sub> (normalized by dividing by three) selectivity was also obtained. Nanosponge-structured electrodes showed higher product selectivity but lower PEC activity than the other nanotube and nanobelt ones.

Pecoraro et al. [148] synthesized nanotube-structured TiO<sub>2</sub> on Ti foil and felt, as photoanode, for simultaneous PEC oxidation of glycerol and H<sub>2</sub> production in water under UV-Vis irradiation. Ni foam was used as the cathode. The initial substrate (glycerol) and electrolyte (Na<sub>2</sub>SO<sub>4</sub>) concentrations, applied potential, and light intensity values are 100 mM, 0.5 M, 1 V, and 10 mW/cm<sup>2</sup>, respectively. The PEC experiments were performed at pH=2, and the photoanode area was 90 cm<sup>2</sup>. Under these conditions, DHA, GDA, and H<sub>2</sub> production rates were 0.0484, 0.134, and 1.67 μmol·h<sup>-1</sup>·mW<sup>-1</sup>, respectively, using the best electrode which was calcined at 450 °C after its production in ethylene glycol.

Jung et al. [149] investigated a Bi-based metal-organic framework decorated WO<sub>3</sub> anode on an FTO surface for selective PEC oxidation of glycerol to GDA under solar light at pH=2 in 0.5 M Na<sub>2</sub>SO<sub>4</sub> electrolyte medium. The catalyst was prepared on the FTO surface by hydro/solvothermal synthesis methods. The GDA production rate using high glycerol concentration (2 M) was 420 mmol·m<sup>-2</sup>·h<sup>-1</sup> at 1.2 V vs RHE after 1h reaction. In addition, selectivity towards GDA at that condition was high (ca. 94%), and a small DHA amount was also observed.

Liu and coworkers [87] achieved selective PEC oxidation of glycerol to DHA by investigating Ag nanoparticle-loaded layered double hydroxide (LDH) nanosheets on TiO<sub>2</sub> nanoarray (Ag@LDH@TiO<sub>2</sub>) under solar irradiation in water at pH=7 in H-type cell. The dominating active oxygen species is the hydroxyl radical generated by water oxidation. It was determined

that the middle hydroxyl group is preferentially adsorbed to Ag-loaded LDH surfaces, and the surface-bound hydroxyl radicals mediated dehydrogenation barriers of middle carbon of adsorbed glycerol. Consequently, Ag@LDH@TiO<sub>2</sub> photoanode gave 72% (carbon balance ca. 95%) selectivity to DHA, while pristine TiO<sub>2</sub> only ca. 24% at 1.2 V. Formic acid was the main product (selectivity: 51%) for pure TiO<sub>2</sub>. Due to the high initial concentration of glycerol (100 mM), the conversion after 4 hours using Ag@LDH@TiO<sub>2</sub> was only 2-3%, but the oxidation rate of glycerol was high, i.e. 315 mmol·m<sup>-2</sup>·h<sup>-1</sup>.

Selective PEC middle hydroxyl group of glycerol adsorption was also achieved on Bi<sub>2</sub>O<sub>3</sub>-incorporated TiO<sub>2</sub> nanorod arrays under solar irradiation at pH=2 by Luo et al. [150]. The mainly formic acid formation was observed on the pristine TiO<sub>2</sub> surface, while the electrochemically Bi<sub>2</sub>O<sub>3</sub> incorporated TiO<sub>2</sub> on the FTO surface produced mainly DHA with 65% selectivity after 50% conversion (initial glycerol concentration: 0.1 M). In the PEC system, simultaneous DHA and H<sub>2</sub> production rates were 11.5 μmol·cm<sup>-2</sup>·h<sup>-1</sup> and 0.32 mL·cm<sup>-2</sup>·h<sup>-1</sup>, respectively. However, if an environmental point of view was considered, highly acidic medium (pH=2) and high electrolyte concentration (0.5 M Na<sub>2</sub>SO<sub>4</sub>) used in this work should be avoided. Unfortunately, most PEC glycerol oxidation work has been performed under these undesirable conditions [87,148,150].

Yu et al. [88] performed PEC glycerol oxidation at near-neutral conditions in water under UV irradiation using home-prepared calcined (at 450 °C) WO<sub>3</sub> deposited on ITO. A commercial catalyst, 5%wt WO<sub>3</sub>/TiO<sub>2</sub>, was also used for the sake of comparison. The calcined and crystalline WO<sub>3</sub> showed better performance than the non-calcined, mainly amorphous one. A high amount of commercially valuable products, DHA and GDA, was obtained with calcined WO<sub>3</sub>, while the amount of these products was low using the commercial 5%wt WO<sub>3</sub>/TiO<sub>2</sub> sample. For instance, total selectivity towards DHA and GDA in the presence of calcined WO<sub>3</sub> was 87-95%. Commercial 5%wt WO<sub>3</sub>/TiO<sub>2</sub>, in fact, produced a high amount of formic acid rather than C<sub>3</sub> compounds. PEC oxidation could occur via direct reaction by photogenerated holes or indirect pathway using some oxidant species like hydroxyl radicals. Direct pathways supply mainly valuable C<sub>3</sub> compounds, while indirect ones give raise mainly to over-oxidation species such as formic acid and CO<sub>2</sub>.

Tateno et al. [151] prepared Ta doped BiVO<sub>4</sub>/WO<sub>3</sub> catalyst on FTO as a photoanode for PEC glycerol oxidation in an acidic medium under visible irradiation. Like other PEC works, simultaneous H<sub>2</sub> production at the cathode was also observed. Initial glycerol concentration was 1 M, and it transformed almost entirely into DHA. Only negligible amounts of GDA and formic acid were detected after 2h of PEC reaction. In addition, by increasing the H<sub>2</sub>SO<sub>4</sub> amount,

Faraday efficiency (FE) also increased; in the presence of 25 or 100 mM of the acid, FEs were 61 and 80%, respectively. The prepared photoanode was stable in 25 mM H<sub>2</sub>SO<sub>4</sub> medium after 2h of PEC reaction, while the BiVO<sub>4</sub> electrode, used for comparison, showed some leaching in the acidic medium. Moreover, the FE of the BiVO<sub>4</sub> electrode was low (41%), although the selectivity towards GDA was also high (ca. 93%).

### 3.5 Glucose

Photoelectrocatalytic GLA synthesis could be performed under mild operative conditions. Tian et al. [152] investigated single atom Pt defective decorated and nanorod structured TiO<sub>2</sub> (rutile) on FTO surface to perform selective PEC oxidation of glucose to GLA under simulated solar light in water at 0.6 V *vs* RHE and in a strongly basic medium (1 M KOH). After 5.5 h PEC reaction, 99% glucose (initially 10 mM) conversion, 84 % GLA, and 9.2 GLU yields were obtained. The preparation and some characterization (SEM, XRD, DRS and XPS) results of the anode are shown in Figure 12. The TiO<sub>2</sub> nanorods on FTO were prepared by hydrothermal method, then calcined in air. The electrochemically obtained defective TiO<sub>2</sub> shows high absorption in the UV-Vis region and the presence of Ti<sup>3+</sup>. After that, a single Pt atom deposition on the TiO<sub>2</sub> surface was applied using the atomic layer deposition method.

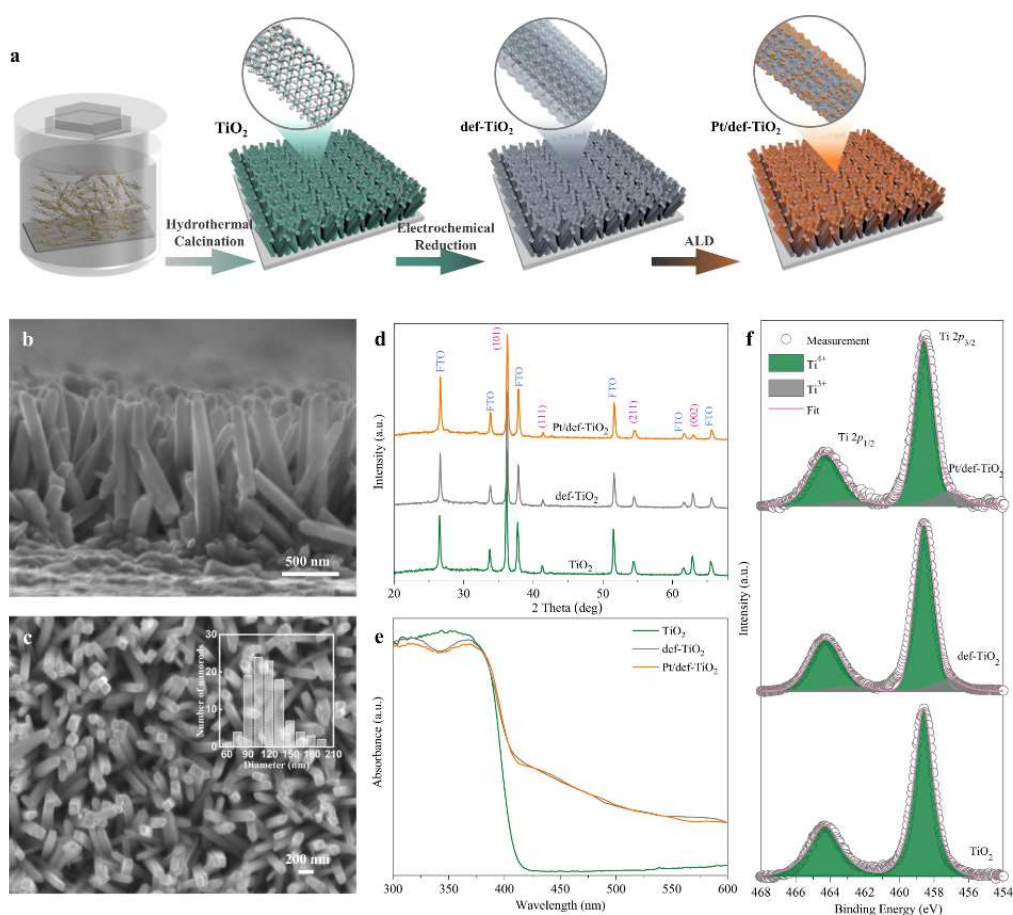


**Figure 12.** a) Schematic illustration of the TiO<sub>2</sub>, defective TiO<sub>2</sub>, and Pt-loaded defective TiO<sub>2</sub> photoanode. b) Top-view and c) side-view SEM images of the nanorod-structured TiO<sub>2</sub> arrays. Inset: the diameter distribution of the TiO<sub>2</sub>. d) XRD patterns, e) UV-vis absorption spectra, and f) XPS spectra of Ti 2p for TiO<sub>2</sub>, defective TiO<sub>2</sub>, and Pt loaded defective TiO<sub>2</sub> [152].

Figure 13 shows a reaction mechanism for PEC oxidation of glucose on a Pt decorated defective TiO<sub>2</sub> surface. Photogenerated holes react with water to produce hydroxyl radicals, which abstract H atoms of the C<sub>1</sub>-H and C<sub>1</sub>-O-H to form C<sub>1</sub>=O in step 2. After that, the C<sub>5</sub>-O bond is broken by hydrolysis, and the GLU molecule is formed through desorption from the anode surface. Pt single atoms selectively adsorb the GLU from the C<sub>6</sub> position (step 4), where the <sup>•</sup>OH radicals could react with the H atoms of C<sub>6</sub>-OH and C<sub>6</sub>-H to form a C<sub>6</sub>=O bond (step 5). In addition, some products desorb from the catalyst to generate glucuronic acid (GUR), and others will adjust their adsorption states for the subsequent reaction. A new C<sub>6</sub>-OH bond could be formed by activating the C<sub>6</sub>=O bond with holes and hydroxyl radicals during step 6. Subsequently, the groups from the C<sub>6</sub> position can follow the same reaction pathway as the C<sub>1</sub> position to yield GLA. Consequently, the single Pt atoms and <sup>•</sup>OH radicals can play critical roles in the partial glucose oxidation to GLA.

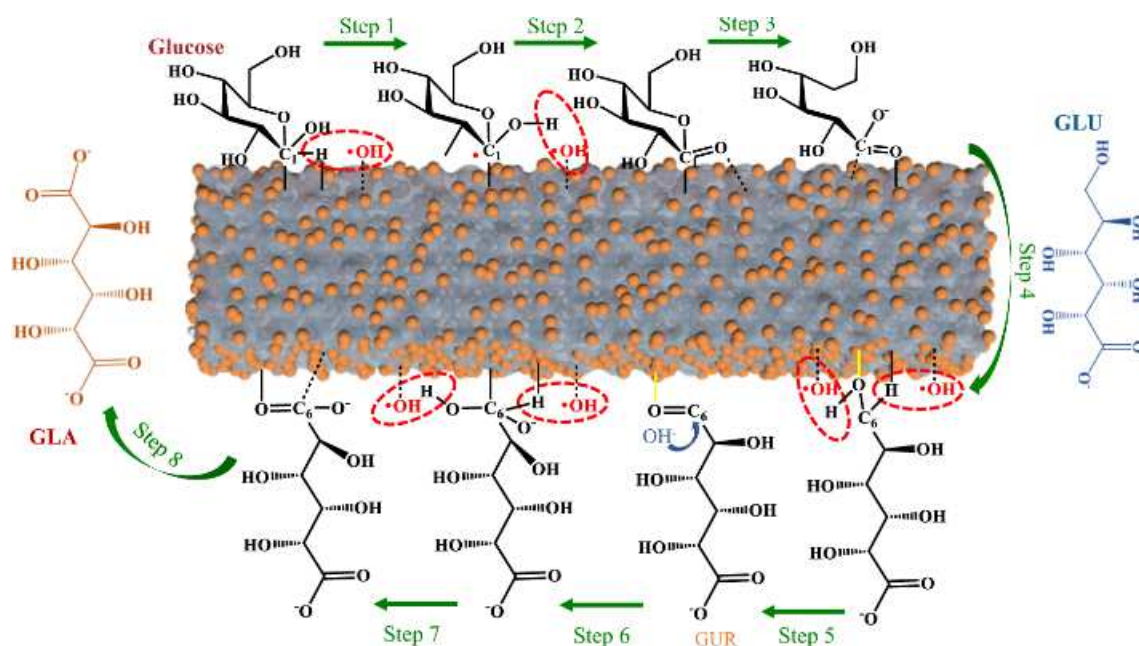


**Figure 13** Schematic illustration of the proposed reaction mechanism of PEC oxidation of glucose into GLA on Pt-loaded defective  $\text{TiO}_2$  [152].

### 3.5 Glyoxal

Glyoxylic acid (GA) was used as a chemical intermediate to synthesize commercially valuable products such as vanillin and penicillin. It could be synthesized by glyoxal oxidation with nitric acid or oxalic acid reduction electrochemically. However, glyoxal oxidation with nitric acid also gives an overoxidation product, oxalic acid. Zhao and co-workers [153] synthesized GA by PEC oxidation of glyoxal in water using  $\text{WO}_3$  nanoplate anodes under simulated solar light at a potential of 1.6 V. The PEC reaction was performed in an acidic medium (in the presence of 0.16 M HCl, at pH 2.8) starting from 100 mM glyoxal. The  $\text{WO}_3$  photoanodes on FTO were prepared by hydrothermal method at 120 °C, following calcination in air at 350-500 °C.  $\text{WO}_3$  catalysts with different quantities of facets ( $\{020\}$ ,  $\{200\}$ , and  $\{002\}$ ) were prepared. However, that containing mainly the  $\{200\}$  facet showed high Faraday efficiency (84%), selectivity towards GA (86.5%), and GA production rate ( $308.4 \text{ mmol m}^{-2} \text{ h}^{-1}$ ) at 1.6V vs RHE after 2h of the PEC reaction. The good results obtained with this material were explained by theoretical calculations as due to its strong glyoxal adsorption capacity and the low energy requirement for the formation of glyoxal radicals on this facet. Moreover, the high energy requirement for GA oxidation to oxalic acid on the  $\{200\}$  facet is the reason for the obtained high selectivity towards GA.

### 3.6 Methanol and butanol

Mesa et al. [154] investigated selective PEC oxidation of methanol to formaldehyde by using  $\text{TiO}_2$  or hematite ( $\alpha\text{-Fe}_2\text{O}_3$ ) under simulated solar irradiation in methanol-water medium. Interestingly, no other products were detected, and selectivity towards formaldehyde was 100%.  $\text{TiO}_2$  catalyst was more effective than hematite for PEC methanol oxidation. The reaction rate mainly depended on the surface hole density and the rate determining step was C-H bond breaking in methanol.

Harris et al. [155] used a biohybrid cell for the PEC transformation of *n*-butanol into *n*-butyraldehyde and 2-ethylhexenal by tandem enzymatic oxidation and aldol condensation at  $\text{pH}=7.5$  under visible irradiation ( $\lambda_{\text{max}}=465 \text{ nm}$ ) with three-electrode system in H-type cell (Figure 14). Alcohol oxidase enzyme transformed *n*-butanol into *n*-butyraldehyde, while the produced  $\text{H}_2\text{O}_2$  oxidized to  $\text{H}^+$  and  $\text{O}_2$  on  $\text{BiVO}_4$  anode. The enzyme activity was protected by  $\text{H}_2\text{O}_2$  oxidation. PEC conversion was higher than the photocatalytic one (6.2 vs. 3.1%). In addition,  $\text{H}_2$  was also produced at cathode surface in the PEC process.

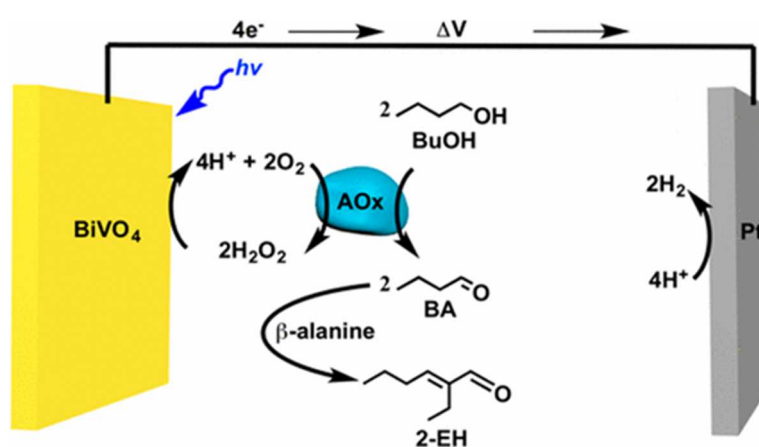


**Figure 14.** Reaction scheme for light-driven oxidation of *n*-butanol to *n*-butyraldehyde and its transformation into 2-ethylhexenal in a biohybrid photoelectrochemical cell [155].

### 3.7 Aromatic and heteroaromatic hydrocarbons

A PEC synthesis study performed simultaneously at both the photoanode and cathode was conducted by Choi et al. [156]. In this PEC system, a Mo-doped  $\text{BiVO}_4$  was used as the anode (only the anode was exposed to solar light), and an inverse opal ITO (IO-ITO) electrode was



used as the cathode that gives rise to the coupling of peroxygenase and ene-reductase-mediated catalysis, respectively. In the PEC cell, the photoexcited electrons generated from the Mo:BiVO<sub>4</sub> were transferred to the IO-ITO and regenerated reduced flavin mononucleotides to drive ene-reductase-catalyzed *trans*-hydrogenation of ketoisophrone to (*R*)-levodione. Meanwhile, the photoactivated Mo:BiVO<sub>4</sub> formed H<sub>2</sub>O<sub>2</sub> in situ via a two-electron water-oxidation process with the aid of an applied bias, which simultaneously supplies peroxygenases to drive selective hydroxylation of ethylbenzene into enantiopure (*R*)-1-phenyl-1-hydroxyethane (see Figure 15).

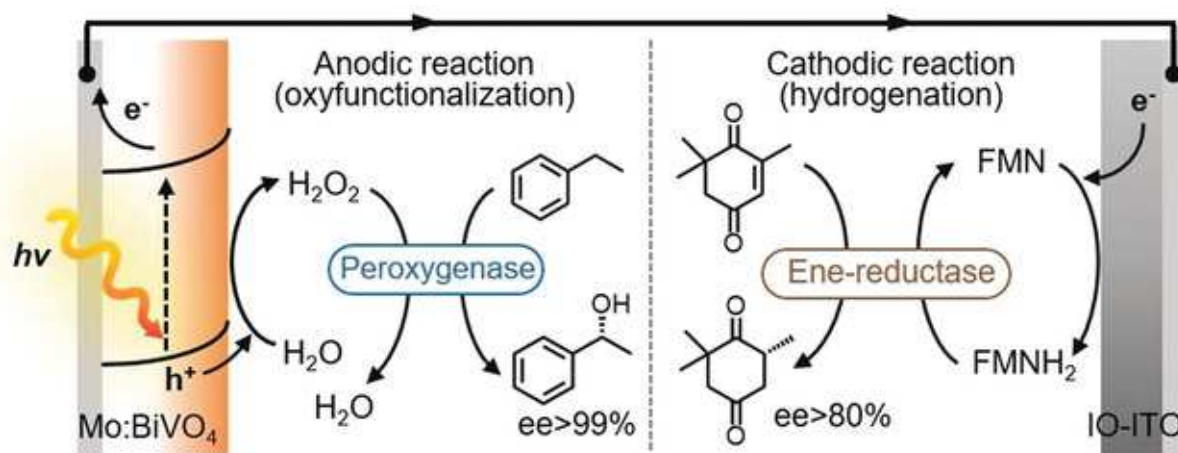
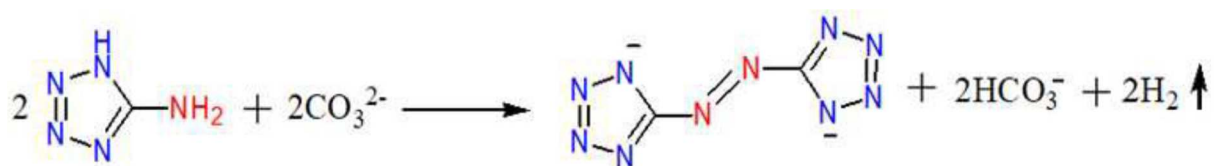


**Figure 15** Schematic illustration of the dual PEC reaction mechanism in the presence of peroxygenase and ene-reductase enzymes using Mo:BiVO<sub>4</sub> and IO-ITO electrodes [156].

5,5'-Azotetrazolate salt derivatives have good thermal stability and low flammability; consequently, they are used in gas generators, propellants, and fireworks in the industry [157,158]. He and co-workers performed the PEC synthesis of sodium 5,5'-azotetrazolate (SZT) from 5-amino-1*H*-tetrazole (Scheme 3) by using W(2%) and Mo(6%) co-doped BiVO<sub>4</sub> photoanode in 0.2 M Na<sub>2</sub>CO<sub>3</sub> medium under simulated solar light [159]. After 8h of PEC reaction, 0.230 mmol SZT was produced (conversion: 11.5%). The same synthesis reaction was also performed with Ti-Fe<sub>2</sub>O<sub>3</sub> film on FTO as the photoanode in 0.1 M NaOH aqueous solution under solar irradiation [160]. The Faraday efficiency of the previous PEC reaction system [159] was higher than the last one (80 vs. 65%) [160]. In addition, the STZ synthesis reaction was also performed in the presence of a magnetic field of 0.5 T as well as irradiation and potential, and about 50% of STZ production increase (18 vs. 27 μmol for 90 min) was obtained.



**Scheme 3.** The PEC synthesis reaction of sodium 5,5'-azotetrazolate (SZT) from 5-amino-1*H*-tetrazole [159].

Tang et al. [161] performed PEC simultaneous synthesis of vitamin B<sub>3</sub> and H<sub>2</sub> from 3-methylpyridine using WO<sub>3</sub> as anode in a dual-chamber quartz cell consisting of a proton exchange membrane under solar irradiation. Selectivity towards vitamin B<sub>3</sub> was high as no other by-product was obtained; however, the PEC reaction was performed in an extremely acidic solution (in 1.5 M H<sub>2</sub>SO<sub>4</sub>); consequently, the process is not environmentally friendly. After 8h of PEC reaction, 60 μmol vitamin B<sub>3</sub> was produced.

Çetinkaya et al. used nanotube-structured TiO<sub>2</sub> decorated with WO<sub>3</sub> on Ti plates to perform the PEC oxidation of 3-methylpyridine in water under UVA irradiation under neutral conditions (pH=7) instead of in the presence of a highly acidic solution [162]. The Ti/TiO<sub>2</sub> plates were prepared in ethylene glycol medium by the anodic oxidation method and calcined at 500 °C. WO<sub>3</sub> decoration significantly increased the yield of vitamin B<sub>3</sub> (ca. 3.0 vs. 50%) with respect to pristine NT-structured TiO<sub>2</sub> under UVA. On the contrary, the reaction rate was low, and no products were obtained under visible light where only unselective photolytic reactions of 3-methylpyridine occurred. In addition, 3-pyridinemethanol, 3-pyridinemethanal, and vitamin B<sub>3</sub> molecules were inactive in a photolytic way since -CH<sub>2</sub>-OH, carbonyl, or -COOH groups in the pyridine ring deactivated the aromatic ring because of their withdrawing effect. In conclusion, PEC and photolytic reactions of 3-methylpyridine occurred competitively under UVA.

A representative experiment of selective PEC oxidation of 3-methylpyridine under UVA light versus time is reported in Figure 16a. The 3-pyridinemethanol concentration is always low during all the time. 3-pyridinemethanal concentration increased and reached a maximum after ca. 95 min, then it decreased due to its transformation into vitamin B<sub>3</sub>. For this reason, selectivity towards vitamin B<sub>3</sub> increased, while those towards 3-pyridinemethanol and 3-pyridinemethanal decreased versus time, and the total product selectivity value was almost constant (62%) during 3h of reaction (see. Figure 16b).

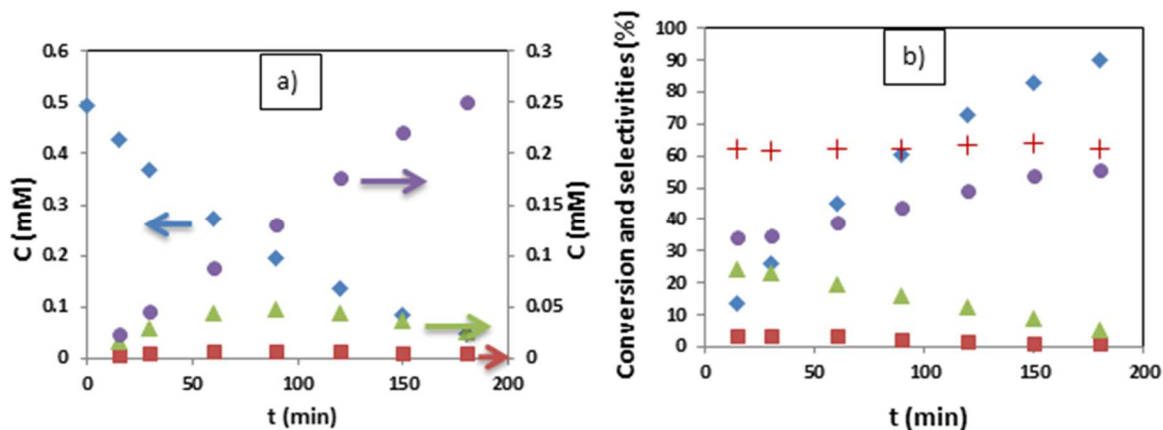


**Fig. 16.** a) A representative experiment of selective PEC oxidation of 3-methylpyridine to 3-pyridinemethanol (■), 3-pyridinemethanol (▲) and vitamin B<sub>3</sub> (●) by using WO<sub>3</sub> decorated electrode in water under UVA versus time. The product concentrations are quoted on the right-hand axes. b) The conversion (◆) and selectivity values of 3-pyridinemethanol (■), 3-pyridinemethanol (▲) and vitamin B<sub>3</sub> (●). +: total selectivity of all three products [162].

## Conclusions and perspectives

In this paper, articles in which the synthesis of valuable molecules was performed in water by heterogeneous photocatalysis and photoelectrocatalysis have been presented and some of them briefly discussed.

Photocatalytic works on this topic involving the use of the photocatalyst in powder or supported form in both discontinuous and continuous systems are very numerous, and it should be noticed that membrane reactors have also been used to achieve high product purity in photocatalytic systems and to achieve intensification of the entire process. High selectivity towards one or more products has been obtained using these technologies generally by carrying out the reactions in organic solvents. However, the use of water as the solvent is the most important parameter for these reactions to be defined as green processes, i.e. environmentally friendly.

Papers on synthesis reactions carried out by photoelectrocatalysis are very few, and notably, only about half of them have been carried out in an aqueous environment. During PEC synthesis reactions, interestingly a simultaneous production of H<sub>2</sub> at the cathode in a separate cell has been reported in some cases. Nevertheless, most of these works were performed at strongly acidic pH's in the presence of high amounts of electrolytes, and these experimental conditions, of course, do not obey the principles of green chemistry. Another weakness is that all these reactions have been carried out in supported fragile anodes, and in small batch systems.

However, photoelectrocatalytic processes could be performed in continuous mode and industrial-scale PEC reactors could also be considered for some niche applications. These systems could, in principle, be coupled with suitable membranes to selectively permeate the

desired product(s). In this way the anodic compartment would remain separated from the cathodic one, avoiding a possible cathodic reduction of the product(s).

We conclude by saying that the study of PEC systems for the selective synthesis of valuable compounds and the simultaneous production of H<sub>2</sub> is in its initial stages. The ideal conditions for a scale-up prior to a possible application are the use of catalysts stably supported in divided cells, a minimum amount of electrolyte, pH conditions close to neutrality and sunlight. However, the authors realize that achieving this objective by optimizing all these parameters is not easy, and readers know well that each type of reaction requires often very different experimental conditions (including the type of reactor).

## References

- [1] K. Nakata, A. Fujishima, TiO<sub>2</sub> photocatalysis: Design and applications, *J. Photochem. Photobiol. C.* 13 (2012) 169–189. <https://doi.org/10.1016/j.jphotochemrev.2012.06.001>.
- [2] A. Mills, S. Le Hunte, An overview of semiconductor photocatalysis, *J. Photochem. Photobiol. A.* 108 (1997) 1-35. [https://doi.org/10.1016/S1010-6030\(97\)00118-4](https://doi.org/10.1016/S1010-6030(97)00118-4).
- [3] M.A. Fox, M. Dulay, Heterogeneous Photocatalysis, *Chem. Rev.* 93 (1993) 341–357. <https://doi.org/10.1021/cr00017a016>.
- [4] J.-M. Herrmann, Heterogeneous photocatalysis: fundamentals and applications to the removal of various types of aqueous pollutants, *Catal. Today*, 53 (1999) 115-129. [https://doi.org/10.1016/S0920-5861\(99\)00107-8](https://doi.org/10.1016/S0920-5861(99)00107-8).
- [5] L.G. Devi, R. Kavitha, A review on non metal ion doped titania for the photocatalytic degradation of organic pollutants under UV/solar light: Role of photogenerated charge carrier dynamics in enhancing the activity, *Appl Catal B.* 140–141 (2013) 559–587. <https://doi.org/10.1016/j.apcatb.2013.04.035>.
- [6] M. Pelaez, N.T. Nolan, S.C. Pillai, M.K. Seery, P. Falaras, A.G. Kontos, P.S.M. Dunlop, J.W.J. Hamilton, J.A. Byrne, K. O’Shea, M.H. Entezari, D.D. Dionysiou, A review on the visible light active titanium dioxide photocatalysts for environmental applications, *Appl. Catal. B.* 125 (2012) 331–349. <https://doi.org/10.1016/j.apcatb.2012.05.036>.
- [7] L. Llatance-Guevara, N.E. Flores, G.O. Barrionuevo, J.L. Mullo Casillas, Waste Biomass Selective and Sustainable Photooxidation to High-Added-Value Products: A Review, *Catalysts.* 12 (2022) 1091. <https://doi.org/10.3390/catal12101091>.
- [8] S. Kampouri, K.C. Stylianou, Dual-Functional Photocatalysis for Simultaneous Hydrogen Production and Oxidation of Organic Substances, *ACS Catal.* 9 (2019) 4247–4270. <https://doi.org/10.1021/acscatal.9b00332>.

- [9] F. Parrino, M. Bellardita, E.I. García-López, G. Marci, V. Loddo, L. Palmisano, Heterogeneous Photocatalysis for Selective Formation of High-Value-Added Molecules: Some Chemical and Engineering Aspects, *ACS Catal.* 8 (2018) 11191–11225. <https://doi.org/10.1021/acscatal.8b03093>.
- [10] M. Bellardita, V. Loddo, G. Palmisano, I. Pibiri, L. Palmisano, V. Augugliaro, Photocatalytic green synthesis of piperonal in aqueous TiO<sub>2</sub> suspension, *Appl. Catal. B.* 144 (2014) 607–613. <https://doi.org/10.1016/j.apcatb.2013.07.070>.
- [11] M. Yamauchi, H. Saito, T. Sugimoto, S. Mori, S. Saito, Sustainable organic synthesis promoted on titanium dioxide using coordinated water and renewable energies/resources, *Coord. Chem. Rev.* 472 (2022). <https://doi.org/10.1016/j.ccr.2022.214773>.
- [12] L. Chen, J. Tang, L.N. Song, P. Chen, J. He, C.T. Au, S.F. Yin, Heterogeneous photocatalysis for selective oxidation of alcohols and hydrocarbons, *Appl. Catal. B.* 242 (2019) 379–388. <https://doi.org/10.1016/j.apcatb.2018.10.025>.
- [13] M. Bellardita, M. Feilizadeh, R. Fiorenza, S. Scirè, L. Palmisano, V. Loddo, Selective aqueous oxidation of aromatic alcohols under solar light in the presence of TiO<sub>2</sub> modified with different metal species, *Photochem. Photobiol. Sci.* 21 (2022) 2139–215. <https://doi.org/10.1007/s43630-022-00284-2>.
- [14] S. Yurdakal, M. Bellardita, I. Pibiri, L. Palmisano, V. Loddo, Aqueous selective photocatalytic oxidation of salicyl alcohol by TiO<sub>2</sub> catalysts: Influence of some physico-chemical features, *Catal Today.* 380 (2021) 16–24. <https://doi.org/10.1016/j.cattod.2021.06.030>.
- [15] X. Li, J.L. Shi, H. Hao, X. Lang, Visible light-induced selective oxidation of alcohols with air by dye-sensitized TiO<sub>2</sub> photocatalysis, *Appl. Catal. B.* 232 (2018) 260–267. <https://doi.org/10.1016/j.apcatb.2018.03.043>.
- [16] J. Kaur, B. Pal, 100% selective yield of m-nitroaniline by rutile TiO<sub>2</sub> and m-phenylenediamine by P25-TiO<sub>2</sub> during m-dinitrobenzene photoreduction, *Catal. Commun.* 53 (2014) 25–28. <https://doi.org/10.1016/j.catcom.2014.04.019>.
- [17] H. Huang, J. Zhou, H. Liu, Y. Zhou, Y. Feng, Selective photoreduction of nitrobenzene to aniline on TiO<sub>2</sub> nanoparticles modified with amino acid, *J. Hazard. Mater.* 178 (2010) 994–998. <https://doi.org/10.1016/j.jhazmat.2010.02.037>.
- [18] Y. Shiraishi, Y. Togawa, D. Tsukamoto, S. Tanaka, T. Hirai, Highly efficient and selective hydrogenation of nitroaromatics on photoactivated rutile titanium dioxide, *ACS Catal.* 2 (2012) 2475–2481. <https://doi.org/10.1021/cs300500p>.
- [19] M. Bellardita, D. Virtù, F. Di Franco, V. Loddo, L. Palmisano, M. Santamaria, Heterogeneous photocatalytic aqueous succinic acid formation from maleic acid reduction, *Chem. Eng. J.* 431 (2022) 134131. <https://doi.org/10.1016/j.cej.2021.134131>.
- [20] M. Bellardita, V. Loddo, L. Palmisano, Formation of High Added Value Chemicals by Photocatalytic Treatment of Biomass, *Mini Rev. Org. Chem.* 17 (2020) 884–901. <https://doi.org/10.2174/1570193x17666200131112856>.

- [21] R. Djellabi, D. Aboagye, M.G. Galloni, V. Vilas Andhalkar, S. Nouacer, W. Nabgan, S. Rtimi, M. Constantí, F. Medina Cabello, S. Contreras, Combined conversion of lignocellulosic biomass into high-value products with ultrasonic cavitation and photocatalytic produced reactive oxygen species – A review, *Bioresour. Technol.* 368 (2023) 128333. <https://doi.org/10.1016/j.biortech.2022.128333>.
- [22] G.C. de Assis, I.M.A. Silva, T.G. dos Santos, T. V. dos Santos, M.R. Meneghetti, S.M.P. Meneghetti, Photocatalytic processes for biomass conversion, *Catal. Sci. Technol.* 11 (2021) 2354–2360. <https://doi.org/10.1039/d0cy02358b>.
- [23] X. Wu, H. Zhao, M.A. Khan, P. Maity, T. Al-Attas, S. Larter, Q. Yong, O.F. Mohammed, M.G. Kibria, J. Hu, Sunlight-Driven Biomass Photorefinery for Coproduction of Sustainable Hydrogen and Value-Added Biochemicals, *ACS Sustain. Chem. Eng.* 8 (2020) 15772–15781. <https://doi.org/10.1021/ACSSUSCHEMENG.0C06282>.
- [24] D. Liang, J. Wu, C. Xie, J. Wen, Y. Lyu, Z. Sofer, J. Zheng, S. Wang, Efficiently and selectively photocatalytic cleavage of C–C bond by C<sub>3</sub>N<sub>4</sub> nanosheets: Defect-enhanced engineering and rational reaction route, *Appl. Catal. B.* 317 (2022) 121690. <https://doi.org/10.1016/j.apcatb.2022.121690>.
- [25] H.J. Lee, E.S. Cho, Selective Photocatalytic C–C Bond Cleavage of Lignin Models and Conversion to High-Value Chemical by Polyoxometalate under a Mild Water-Based Environment, *ACS Sustain. Chem. Eng.* 11 (2023) 7624–7632. <https://doi.org/10.1021/acssuschemeng.2c06011>.
- [26] O. Ola, M.M. Maroto-Valer, Review of material design and reactor engineering on TiO<sub>2</sub> photocatalysis for CO<sub>2</sub> reduction, *J. Photochem. Photobiol. C.* 24 (2015) 16–42. <https://doi.org/10.1016/j.jphotochemrev.2015.06.001>.
- [27] R. Fiorenza, M. Bellardita, S.A. Balsamo, A. Gulino, M. Condorelli, G. Compagnini, S. Scirè, L. Palmisano, A solar photothermo-catalytic combined process for the VOCs combustion and the subsequent CO<sub>2</sub> valorization using noble metal-free catalysts, *Catal. Today.* 413-415 (2022) 113949. <https://doi.org/10.1016/j.cattod.2022.11.010>.
- [28] M. Bellardita, A. Di Paola, E. García-López, V. Loddo, G. Marci, L. Palmisano, Photocatalytic CO<sub>2</sub> Reduction in Gas-Solid Regime in the Presence of Bare, SiO<sub>2</sub> Supported or Cu-Loaded TiO<sub>2</sub> Samples, 17 (2013) 2440-2448. <https://dx.doi.org/10.2174/13852728113179990057>
- [29] A. Nikokavoura, C. Trapalis, Alternative photocatalysts to TiO<sub>2</sub> for the photocatalytic reduction of CO<sub>2</sub>, *Appl. Surf. Sci.* 391 (2017) 149–174. <https://doi.org/10.1016/j.apsusc.2016.06.172>.
- [30] M. Ni, M.K.H. Leung, D.Y.C. Leung, K. Sumathy, A review and recent developments in photocatalytic water-splitting using TiO<sub>2</sub> for hydrogen production, *Renew. Sustain. Energy Rev.* 11 (2007) 401–425. <https://doi.org/10.1016/j.rser.2005.01.009>.
- [31] C.H. Liao, C.W. Huang, J.C.S. Wu, Hydrogen production from semiconductor-based photocatalysis via water splitting, *Catalysts.* 2 (2012) 490–516. <https://doi.org/10.3390/catal2040490>.

- [32] E. Wierzbicka, M. Altomare, M. Wu, N. Liu, T. Yokosawa, D. Fehn, S. Qin, K. Meyer, T. Unruh, E. Spiecker, L. Palmisano, M. Bellardita, J. Will, P. Schmuki, Reduced grey brookite for noble metal free photocatalytic H<sub>2</sub> evolution, *J. Mater. Chem. A Mater.* 9 (2021) 1168–1179. <https://doi.org/10.1039/d0ta09066b>.
- [33] R. Fiorenza, S. Sciré, L. D’Urso, G. Compagnini, M. Bellardita, L. Palmisano, Efficient H<sub>2</sub> production by photocatalytic water splitting under UV or solar light over variously modified TiO<sub>2</sub>-based catalysts, *Int. J. Hydrogen Energy.* 44 (2019) 14796–14807. <https://doi.org/10.1016/j.ijhydene.2019.04.035>.
- [34] J.C. Colmenares, A. Magdziarz, M.A. Aramendia, A. Marinas, J.M. Marinas, F.J. Urbano, J.A. Navio, Influence of the strong metal support interaction effect (SMSI) of Pt/TiO<sub>2</sub> and Pd/TiO<sub>2</sub> systems in the photocatalytic biohydrogen production from glucose solution, *Catal. Commun.* 16 (2011) 1–6. <https://doi.org/10.1016/j.catcom.2011.09.003>.
- [35] Y.H. Zhang, M.M. Liu, J.L. Chen, K.F. Xie, S.M. Fang, Dendritic branching Z-scheme Cu<sub>2</sub>O/TiO<sub>2</sub> heterostructure photocatalysts for boosting H<sub>2</sub> production, *J. Phys. Chem. Solids.* 152 (2021) 109948. <https://doi.org/10.1016/j.jpcs.2021.109948>.
- [36] M. Bellardita, V. Loddo, F. Parrino, L. Palmisano, (Photo)electrocatalytic Versus Heterogeneous Photocatalytic Carbon Dioxide Reduction, *ChemPhotoChem.* 5 (2021) 767–791. <https://doi.org/10.1002/cptc.202100030>.
- [37] P. Lianos, Review of recent trends in photoelectrocatalytic conversion of solar energy to electricity and hydrogen, *Appl. Catal. B.* 210 (2017) 235–254. <https://doi.org/10.1016/j.apcatb.2017.03.067>.
- [38] S.Y. Li, K.F. Huang, Z.Y. Tang, J.H. Wang, Photoelectrocatalytic organic synthesis: a versatile method for the green production of building-block chemicals, *J. Mater. Chem. A.* 11 (2023) 3281–3296. <https://doi.org/10.1039/d2ta09430d>.
- [39] Photoelectrocatalysis: Fundamental and Applications. L. Palmisano and S. Yurdakal Eds, . (2023). <https://doi.org/10.1016/B978-0-12-823989-6.09989-6>.
- [40] G.G. Bessegato, T.T. Guaraldo, J.F. de Brito, M.F. Brugnera, M.V.B. Zanoni, Achievements and Trends in Photoelectrocatalysis: from Environmental to Energy Applications, *Electrocatalysis.* 6 (2015) 415–441. <https://doi.org/10.1007/s12678-015-0259-9>.
- [41] C. Durante, M. Mazzucato, M. Bellardita, F. Parrino, Fundamentals of photoelectrocatalysis, *Photoelectrocatalysis: Fundamentals and Applications.* (2023) 7–81. <https://doi.org/10.1016/B978-0-12-823989-6.00003-5>.
- [42] S. Yurdakal, O. Alagöz, L. Özcan, L. Palmisano, Selective photoelectrocatalytic transformations of organic compounds, *Photoelectrocatalysis: Fundamentals and Applications.* (2023) 361–420. <https://doi.org/10.1016/B978-0-12-823989-6.00001-1>.
- [43] Y. Wang, M. Zu, X. Zhou, H. Lin, F. Peng, S. Zhang, Designing efficient TiO<sub>2</sub>-based photoelectrocatalysis systems for chemical engineering and sensing, *Chem. Eng. J.* 381 (2020) 122605. <https://doi.org/10.1016/j.cej.2019.122605>.

- [44] G. Palmisano, S. Yurdakal, V. Augugliaro, V. Loddo, L. Palmisano, Photocatalytic selective oxidation of 4-methoxybenzyl alcohol to aldehyde in aqueous suspension of home-prepared titanium dioxide catalyst, *Adv. Synth. Catal.* 349 (2007) 964–970. <https://doi.org/10.1002/adsc.200600435>.
- [45] M. Addamo, V. Augugliaro, A. Di Paola, E. García-López, V. Loddo, G. Marci, L. Palmisano, Preparation and photoactivity of nanostructured TiO<sub>2</sub> particles obtained by hydrolysis of TiCl<sub>4</sub>, *Colloids Surf. A Physicochem. Eng Asp.* 265 (2005) 23–31. <https://doi.org/10.1016/j.colsurfa.2004.11.048>.
- [46] M. Addamo, V. Augugliaro, M. Bellardita, A. Di Paola, V. Loddo, G. Palmisano, L. Palmisano, S. Yurdakal, Environmentally friendly photocatalytic oxidation of aromatic alcohol to aldehyde in aqueous suspension of brookite TiO<sub>2</sub>, *Catal Letters.* 126 (2008) 58–62. <https://doi.org/10.1007/s10562-008-9596-0>.
- [47] S. Yurdakal, G. Palmisano, V. Loddo, V. Augugliaro, L. Palmisano, Nanostructured rutile TiO<sub>2</sub> for selective photocatalytic oxidation of aromatic alcohols to aldehydes in water, *J Am Chem Soc.* 130 (2008) 1568–1569. <https://doi.org/10.1021/ja709989e>.
- [48] S. Yurdakal, G. Palmisano, V. Loddo, O. Alagöz, V. Augugliaro, L. Palmisano, Selective photocatalytic oxidation of 4-substituted aromatic alcohols in water with rutile TiO<sub>2</sub> prepared at room temperature, *Green Chemistry.* 11 (2009) 510–51. <https://doi.org/10.1039/b819862d>.
- [49] A. Di Paola, M. Bellardita, L. Palmisano, Z. Barbieriková, V. Brezová, Influence of crystallinity and OH surface density on the photocatalytic activity of TiO<sub>2</sub> powders, *J. Photochem. Photobiol. A.* 273 (2014) 59–67. <https://doi.org/10.1016/j.jphotochem.2013.09.008>.
- [50] S. Yurdakal, V. Augugliaro, V. Loddo, G. Palmisano, L. Palmisano, Enhancing selectivity in photocatalytic formation of p-anisaldehyde in aqueous suspension under solar light irradiation via TiO<sub>2</sub> N-doping, *New Journal of Chemistry.* 36 (2012) 1762–1768. <https://doi.org/10.1039/c2nj40394c>.
- [51] M. Bellardita, C. Garlisi, A.M. Venezia, G. Palmisano, L. Palmisano, Influence of fluorine on the synthesis of anatase TiO<sub>2</sub> for photocatalytic partial oxidation: Are exposed facets the main actors?, *Catal Sci Technol.* 8 (2018) 1606–1620. <https://doi.org/10.1039/c7cy02382k>.
- [52] M. D'Arienzo, J. Carbajo, A. Bahamonde, M. Crippa, S. Polizzi, R. Scotti, L. Wahba, F. Morazzoni, Photogenerated defects in shape-controlled TiO<sub>2</sub> anatase nanocrystals: A probe to evaluate the role of crystal facets in photocatalytic processes, *J. Am. Chem. Soc.* 133 (2011) 17652–17661. <https://doi.org/10.1021/ja204838s>.
- [53] G. Liu, J.C. Yu, G.Q. Lu, H.M. Cheng, Crystal facet engineering of semiconductor photocatalysts: Motivations, advances and unique properties, *Chemical Communications.* 47 (2011) 6763–6783. <https://doi.org/10.1039/c1cc10665a>.
- [54] T. Butburee, P. Kotchasarn, P. Hirunsit, Z. Sun, Q. Tang, P. Khemthong, W. Sangkhun, W. Thongsuwan, P. Kumnorkaew, H. Wang, K. Faungnawakij, New understanding of crystal



- control and facet selectivity of titanium dioxide ruling photocatalytic performance, *J. Mater. Chem. A*. 7 (2019) 8156–8166. <https://doi.org/10.1039/c8ta11475g>.
- [55] M. Maisano, M.V. Dozzi, M. Coduri, L. Artiglia, G. Granozzi, E. Selli, Unraveling the Multiple Effects Originating the Increased Oxidative Photoactivity of {001}-Facet Enriched Anatase TiO<sub>2</sub>, *ACS Appl. Mater. Interfaces*. 8 (2016) 9745–9754. <https://doi.org/10.1021/acsami.6b01808>.
- [56] H. Zhang, X. Liu, Y. Li, Y. Li, H. Zhao, {001} facets dominated anatase TiO<sub>2</sub>: Morphology, formation/etching mechanisms and performance, *Sci China Chem*. 56 (2013) 402–417. <https://doi.org/10.1007/s11426-012-4766-8>.
- [57] M. Bellardita, G. Escolano-Casado, L. Palmisano, L. Mino, Surface processes in selective photocatalytic oxidation of hydroxybenzyl alcohols by TiO<sub>2</sub> P25, *Catal. Today*. 413-415 (2022) 113983. <https://doi.org/10.1016/j.cattod.2022.12.014>.
- [58] D. Tsukamoto, M. Ikeda, Y. Shiraishi, T. Hara, N. Ichikuni, S. Tanaka, T. Hirai, Selective photocatalytic oxidation of alcohols to aldehydes in water by TiO<sub>2</sub> partially coated with WO<sub>3</sub>, *Chemistry - A European Journal*. 17 (2011) 9816–9824. <https://doi.org/10.1002/chem.201100166>.
- [59] A.M. Djaballah, M. Bellardita, L. Palmisano, V. Loddo, M. Umair, C.M. Pecoraro, R. Bagtache, M. Trari, Facile preparation of CuBi<sub>2</sub>O<sub>4</sub>/TiO<sub>2</sub> hetero-systems employed for simulated solar-light selective oxidation of 4-methoxybenzyl alcohol model compound, *Mol. Catal*. 546 (2023) 113251. <https://doi.org/10.1016/j.mcat.2023.113251>.
- [60] F. Li, Y. Wang, J. Du, Y. Zhu, C. Xu, L. Sun, Simultaneous oxidation of alcohols and hydrogen evolution in a hybrid system under visible light irradiation, *Appl. Catal. B*. 225 (2018) 258–263. <https://doi.org/10.1016/j.apcatb.2017.11.072>.
- [61] M. Bellardita, E.I. García-López, G. Marci, I. Krivtsov, J.R. García, L. Palmisano, Selective photocatalytic oxidation of aromatic alcohols in water by using P-doped g-C<sub>3</sub>N<sub>4</sub>, *Appl. Catal. B*. 220 (2018) 222–233. <https://doi.org/10.1016/j.apcatb.2017.08.033>.
- [62] M.J. Sampaio, A. Benyounes, P. Serp, J.L. Faria, C.G. Silva, Photocatalytic synthesis of vanillin using N-doped carbon nanotubes/ZnO catalysts under UV-LED irradiation, *Appl. Catal. A*. 551 (2018) 71–78. <https://doi.org/10.1016/j.apcata.2017.12.002>.
- [63] R. Du, C. Wang, L. Guo, R.A. Soomro, B. Xu, C. Yang, F. Fu, D. Wang, NiS/Cd<sub>0.6</sub>Zn<sub>0.4</sub>S Schottky Junction Bifunctional Photocatalyst for Sunlight-Driven Highly Selective Catalytic Oxidation of Vanillyl Alcohol Towards Vanillin Coupled with Hydrogen Evolution Reaction, *Small*. 19 (2023) 2302330. <https://doi.org/10.1002/sml.202302330>.
- [64] A. Tanaka, K. Hashimoto, H. Kominami, Selective photocatalytic oxidation of aromatic alcohols to aldehydes in an aqueous suspension of gold nanoparticles supported on cerium(IV) oxide under irradiation of green light, *Chem. Commun*. 47 (2011) 10446–10448. <https://doi.org/10.1039/c1cc13801d>.

- [65] X. Xu, L. Shi, S. Zhang, Z. Ao, J. Zhang, S. Wang, H. Sun, Photocatalytic reforming of lignocellulose: A review, *Chem. Eng. J.* 469 (2023) 143972. <https://doi.org/10.1016/j.cej.2023.143972>.
- [66] M. Wang, H. Zhou, F. Wang, Photocatalytic Production of Syngas from Biomass, *Acc. Chem. Res.* 56 (2023) 1057–1069. <https://doi.org/10.1021/acs.accounts.3c00039>.
- [67] A. Negi, K.K. Kesari, Light-Driven Depolymerization of Cellulosic Biomass into Hydrocarbons, *Polymers (Basel)*. 15 (2023) 3671. <https://doi.org/10.3390/polym15183671>.
- [68] R. Jaswal, R. Shende, W. Nan, A. Shende, Photocatalytic reforming of pinewood (*Pinus ponderosa*) acid hydrolysate for hydrogen generation, *Int. J. Hydrogen Energy*. 42 (2017) 2839–2848. <https://doi.org/10.1016/j.ijhydene.2016.12.006>.
- [69] C.M. Pecoraro, M. Bellardita, V. Loddo, D. Virtù, F. Di Franco, M. Santamaria, Photocatalytic and photoelectrocatalytic H<sub>2</sub> evolution combined with valuable furfural production, *Appl. Catal. A*. 650 (2023) 118987. <https://doi.org/10.1016/j.apcata.2022.118987>.
- [70] C.M. Pecoraro, M. Bellardita, V. Loddo, F. Di Franco, L. Palmisano, M. Santamaria, A facile way to synthesize noble metal free TiO<sub>2</sub> based catalysts for glycerol photoreforming, *J. Ind. Eng. Chem.* 118 (2023) 247–258. <https://doi.org/10.1016/j.jiec.2022.11.010>.
- [71] K.A. Davis, S. Yoo, E.W. Shuler, B.D. Sherman, S. Lee, G. Leem, Photocatalytic hydrogen evolution from biomass conversion, *Nano Converg.* 8 (2021). <https://doi.org/10.1186/s40580-021-00256-9>.
- [72] Kawai, T., Sakata, T. Conversion of carbohydrate into hydrogen fuel by a photocatalytic process, *Nature* 286 (1980) 474–476. <https://doi.org/10.1038/286474a0>.
- [73] X. Tong, Y. Ma, Y. Li, Biomass into chemicals: Conversion of sugars to furan derivatives by catalytic processes, *Appl. Catal. A*. 385 (2010) 1–13. <https://doi.org/10.1016/j.apcata.2010.06.049>.
- [74] L. Filiciotto, A.M. Balu, J.C. Van der Waal, R. Luque, Catalytic insights into the production of biomass-derived side products methyl levulinate, furfural and humins, *Catal Today*. 302 (2018) 2–15. <https://doi.org/10.1016/j.cattod.2017.03.008>.
- [75] Y. Lu, X.Y. Wei, Z. Wen, H.B. Chen, Y.C. Lu, Z.M. Zong, J.P. Cao, S.C. Qi, S.Z. Wang, L.C. Yu, W. Zhao, X. Fan, Y.P. Zhao, Photocatalytic depolymerization of rice husk over TiO<sub>2</sub> with H<sub>2</sub>O<sub>2</sub>, *Fuel Process. Technol.* 117 (2014) 8–16. <https://doi.org/10.1016/J.FUPROC.2013.04.001>.
- [76] H. Li, Z. Lei, C. Liu, Z. Zhang, B. Lu, Photocatalytic degradation of lignin on synthesized Ag-AgCl/ZnO nanorods under solar light and preliminary trials for methane fermentation, *Bioresour Technol.* 175 (2015) 494–501. <https://doi.org/10.1016/j.biortech.2014.10.143>.
- [77] J. Gong, A. Imbault, R. Farnood, The promoting role of bismuth for the enhanced photocatalytic oxidation of lignin on Pt-TiO<sub>2</sub> under solar light illumination, *Appl Catal B*. 204 (2017) 296–303. <https://doi.org/10.1016/j.apcatb.2016.11.045>.

- [78] N. Srisasiwimon, S. Chuangchote, N. Laosiripojana, T. Sagawa, TiO<sub>2</sub>/Lignin-Based Carbon Compositated Photocatalysts for Enhanced Photocatalytic Conversion of Lignin to High Value Chemicals, *ACS Sustain. Chem. Eng.* 6 (2018) 13968–13976. <https://doi.org/10.1021/acssuschemeng.8b02353>.
- [79] C. Shi, F. Kang, Y. Zhu, M. Teng, J. Shi, H. Qi, Z. Huang, C. Si, F. Jiang, J. Hu, Photoreforming lignocellulosic biomass for hydrogen production: Optimized design of photocatalyst and photocatalytic system, *Chem. Eng. J.* 452 (2023) 138980. <https://doi.org/10.1016/j.cej.2022.138980>.
- [80] D.W. Wakerley, M.F. Kuehnel, K.L. Orchard, K.H. Ly, T.E. Rosser, E. Reisner, Solar-driven reforming of lignocellulose to H<sub>2</sub> with a CdS/CdO<sub>x</sub> photocatalyst, *Nat. Energy.* 2 (2017) 17021. <https://doi.org/10.1038/nenergy.2017.21>.
- [81] L. Zhang, W. Wang, S. Zeng, Y. Su, H. Hao, Enhanced H<sub>2</sub> evolution from photocatalytic cellulose conversion based on graphitic carbon layers on TiO<sub>2</sub>/NiO<sub>x</sub>, *Green Chemistry.* 20 (2018) 3008–3013. <https://doi.org/10.1039/c8gc01398e>.
- [82] J. Zou, G. Zhang, X. Xu, One-pot photoreforming of cellulosic biomass waste to hydrogen by merging photocatalysis with acid hydrolysis, *Appl Catal A Gen.* 563 (2018) 73–79. <https://doi.org/10.1016/j.apcata.2018.06.030>.
- [83] A. Speltini, M. Sturini, D. Dondi, E. Annovazzi, F. Maraschi, V. Caratto, A. Profumo, A. Buttafava, Sunlight-promoted photocatalytic hydrogen gas evolution from water-suspended cellulose: A systematic study, *Photochemical and Photobiological Sciences.* 13 (2014) 1410–1419. <https://doi.org/10.1039/c4pp00128a>.
- [84] C. Li, H. Wang, S.B. Naghadeh, J.Z. Zhang, P. Fang, Visible light driven hydrogen evolution by photocatalytic reforming of lignin and lactic acid using one-dimensional NiS/CdS nanostructures, *Appl Catal B.* 227 (2018) 229–239. <https://doi.org/10.1016/j.apcatb.2018.01.038>.
- [85] M. Anitha, S.K. Kamarudin, N.T. Kofli, The potential of glycerol as a value-added commodity, *Chemical Engineering Journal.* 295 (2016) 119–130. <https://doi.org/10.1016/j.cej.2016.03.012>.
- [86] S. Bagheri, N.M. Julkapli, W.A. Yehye, Catalytic conversion of biodiesel derived raw glycerol to value added products, *Renewable and Sustainable Energy Reviews.* 41 (2015) 113–127. <https://doi.org/10.1016/j.rser.2014.08.031>.
- [87] Y. Liu, M. Wang, B. Zhang, D. Yan, X. Xiang, Mediating the Oxidizing Capability of Surface-Bound Hydroxyl Radicals Produced by Photoelectrochemical Water Oxidation to Convert Glycerol into Dihydroxyacetone, *ACS Catal.* 12 (2022) 6946–6957. <https://doi.org/10.1021/acscatal.2c01319>.
- [88] J. Yu, J. González-Cobos, F. Dappozze, F.J. López-Tenllado, J. Hidalgo-Carrillo, A. Marinas, P. Vernoux, A. Caravaca, C. Guillard, WO<sub>3</sub>-based materials for photoelectrocatalytic glycerol

- upgrading into glyceraldehyde: Unravelling the synergistic photo- and electro-catalytic effects, *Appl Catal B*. 318 (2022). <https://doi.org/10.1016/j.apcatb.2022.121843>.
- [89] V. Maurino, A. Bedini, M. Minella, F. Rubertelli, E. Pelizzetti, C. Minero, Glycerol Transformation Through Photocatalysis: A Possible Route to Value Added Chemicals, *J. Adv. Oxid. Technol.* 11 (2008). <http://www.environmentalchemistry.unito.it>.
- [90] V. Augugliaro, H.A.H. El Nazer, V. Loddo, A. Mele, G. Palmisano, L. Palmisano, S. Yurdakal, Partial photocatalytic oxidation of glycerol in TiO<sub>2</sub> water suspensions, *Catal Today*. 151 (2010) 21–28. <https://doi.org/10.1016/j.cattod.2010.01.022>.
- [91] L. Guo, Q. Sun, K. Marcus, Y. Hao, J. Deng, K. Bi, Y. Yang, Photocatalytic glycerol oxidation on AuxCu-CuS@TiO<sub>2</sub> plasmonic heterostructures, *J Mater Chem A Mater*. 6 (2018) 22005–22012. <https://doi.org/10.1039/c8ta02170h>.
- [92] P. Limpachanangkul, T. Jedsukontorn, G. Zhang, L. Liu, M. Hunsom, B. Chalermssinuwana, Comparative photocatalytic behavior of photocatalysts (TiO<sub>2</sub>, SiC, Bi<sub>2</sub>O<sub>3</sub>, ZnO) for transformation of glycerol to value added compounds, *Korean Journal of Chemical Engineering*. 36 (2019) 1527–1535. <https://doi.org/10.1007/s11814-019-0326-7>.
- [93] Y. Zhang, N. Zhang, Z.R. Tang, Y.J. Xu, Identification of Bi<sub>2</sub>WO<sub>6</sub> as a highly selective visible-light photocatalyst toward oxidation of glycerol to dihydroxyacetone in water, *Chem Sci*. 4 (2013) 1820–1824. <https://doi.org/10.1039/c3sc50285f>.
- [94] Y. Zhang, R. Ciriminna, G. Palmisano, Y.J. Xu, M. Pagliaro, Sol-gel entrapped visible light photocatalysts for selective conversions, *RSC Adv*. 4 (2014) 18341–18346. <https://doi.org/10.1039/c4ra01031k>.
- [95] S. Zhao, Z. Dai, W. Guo, F. Chen, Y. Liu, R. Chen, Highly selective oxidation of glycerol over Bi/Bi<sub>3.64</sub>Mo<sub>0.36</sub>O<sub>6.55</sub> heterostructure: Dual reaction pathways induced by photogenerated  $1O_2$  and holes, *Appl Catal B*. 244 (2019) 206–214. <https://doi.org/10.1016/j.apcatb.2018.11.047>.
- [96] R. Chong, J. Li, X. Zhou, Y. Ma, J. Yang, L. Huang, H. Han, F. Zhang, C. Li, Selective photocatalytic conversion of glycerol to hydroxyacetaldehyde in aqueous solution on facet tuned TiO<sub>2</sub>-based catalysts, *Chemical Communications*. 50 (2014) 165–167. <https://doi.org/10.1039/c3cc46515b>.
- [97] V. Maslova, A. Fasolini, M. Offidani, S. Albonetti, F. Basile, Solar-driven valorization of glycerol towards production of chemicals and hydrogen, *Catal Today*. 380 (2021) 147–155. <https://doi.org/10.1016/j.cattod.2021.03.008>.
- [98] V. Maslova, E.A. Quadrelli, P. Gaval, A. Fasolini, S. Albonetti, F. Basile, Highly-dispersed ultrafine Pt nanoparticles on microemulsion-mediated TiO<sub>2</sub> for production of hydrogen and valuable chemicals via oxidative photo-dehydrogenation of glycerol, *J Environ Chem Eng*. 9 (2021). <https://doi.org/10.1016/j.jece.2021.105070>.

- [99] M. Bellardita, E.I. García-López, G. Marci, L. Palmisano, Photocatalytic formation of H<sub>2</sub> and value-added chemicals in aqueous glucose (Pt)-TiO<sub>2</sub> suspension, *Int J Hydrogen Energy*. 41 (2016) 5934–5947. <https://doi.org/10.1016/j.ijhydene.2016.02.103>.
- [100] R. Chong, J. Li, Y. Ma, B. Zhang, H. Han, C. Li, Selective conversion of aqueous glucose to value-added sugar aldose on TiO<sub>2</sub>-based photocatalysts, *J Catal*. 314 (2014) 101–108. <https://doi.org/10.1016/j.jcat.2014.03.009>.
- [101] L. Da Vià, C. Recchi, E.O. Gonzalez-Yañez, T.E. Davies, J.A. Lopez-Sanchez, Visible light selective photocatalytic conversion of glucose by TiO<sub>2</sub>, *Appl Catal B*. 202 (2017) 281–288. <https://doi.org/10.1016/j.apcatb.2016.08.035>.
- [102] M. Bellardita, H.A.E. Nazer, V. Loddo, F. Parrino, A.M. Venezia, L. Palmisano, Photoactivity under visible light of metal loaded TiO<sub>2</sub> catalysts prepared by low frequency ultrasound treatment, *Catal Today*. 284 (2017) 92–99. <https://doi.org/10.1016/j.cattod.2016.11.026>.
- [103] M. Bellardita, E.I. García-López, G. Marci, G. Nasillo, L. Palmisano, Photocatalytic Solar Light H<sub>2</sub> Production by Aqueous Glucose Reforming, *Eur J Inorg Chem*. 2018 (2018) 4522–4532. <https://doi.org/10.1002/EJIC.201800663>.
- [104] U. Nwosu, H. Zhao, M. Kibria, J. Hu, Unlocking Selective Pathways for Glucose Photoreforming by Modulating Reaction Conditions, *ACS Sustain Chem Eng*. (2021). <https://doi.org/10.1021/acssuschemeng.1c08708>.
- [105] Y. Ge, Q. Zhang, C. Yang, B. Zhang, K. Deng, Efficient visible-light-driven selective conversion of glucose to high-value chemicals over Bi<sub>2</sub>WO<sub>6</sub>/Co-thioporphyrazine composite in aqueous media, *Appl Catal A Gen*. 623 (2021). <https://doi.org/10.1016/j.apcata.2021.118265>.
- [106] X. Bai, Q. Hou, H. Qian, Y. Nie, T. Xia, R. Lai, G. Yu, M. Laiq Ur Rehman, H. Xie, M. Ju, Selective oxidation of glucose to gluconic acid and glucaric acid with chlorin e6 modified carbon nitride as metal-free photocatalyst, *Appl Catal B*. 303 (2022). <https://doi.org/10.1016/j.apcatb.2021.120895>.
- [107] T.W. Wang, Z.W. Yin, Y.H. Guo, F.Y. Bai, J. Chen, W. Dong, J. Liu, Z.Y. Hu, L. Chen, Y. Li, B.L. Su, Highly Selective Photocatalytic Conversion of Glucose on Holo-Symmetrically Spherical Three-Dimensionally Ordered Macroporous Heterojunction Photonic Crystal, *CCS Chemistry*. 5 (2023) 1773–1788. <https://doi.org/10.31635/ccschem.022.202202213>.
- [108] H.J. Qin, Y.H. Zhang, Z. Wang, G.H. Yang, Photocatalytic Conversion of Fructose to Lactic Acid by BiOBr/Zn@SnO<sub>2</sub> Material, *Catalysts*. 12 (2022). <https://doi.org/10.3390/catal12070719>.
- [109] A. Lolli, V. Maslova, D. Bonincontro, F. Basile, S. Orтели, S. Albonetti, Selective oxidation of HMF via catalytic and photocatalytic processes using metal-supported catalysts, *Molecules*. 23 (2018). <https://doi.org/10.3390/molecules23112792>.
- [110] C. Li, J. Li, L. Qin, P. Yang, D.G. Vlachos, Recent Advances in the Photocatalytic Conversion of Biomass-Derived Furanic Compounds, *ACS Catal*. 11 (2021) 11336–11359. <https://doi.org/10.1021/acscatal.1c02551>.

- [111] X. Tong, Y. Ma, Y. Li, Biomass into chemicals: Conversion of sugars to furan derivatives by catalytic processes, *Appl Catal A Gen.* 385 (2010) 1–13. <https://doi.org/10.1016/j.apcata.2010.06.049>.
- [112] J.J. Bozell, G.R. Petersen, Technology development for the production of biobased products from biorefinery carbohydrates—the US Department of Energy’s “top 10” revisited, *Green Chemistry.* 12 (2010) 539–55. <https://doi.org/10.1039/b922014c>.
- [113] S. Yurdakal, B.S. Tek, O. Alagöz, V. Augugliaro, V. Loddo, G. Palmisano, L. Palmisano, Photocatalytic selective oxidation of 5-(hydroxymethyl)-2-furaldehyde to 2,5-furandicarbaldehyde in water by using anatase, rutile, and brookite TiO<sub>2</sub> nanoparticles, *ACS Sustain Chem Eng.* 1 (2013) 456–461. <https://doi.org/10.1021/sc300142a>.
- [114] A. Ulyankina, S. Mitchenko, N. Smirnova, Selective photocatalytic oxidation of 5-HMF in water over electrochemically synthesized TiO<sub>2</sub> nanoparticles, *Processes.* 8 (2020). <https://doi.org/10.3390/pr8060647>.
- [115] W. Zhang, X. Li, S. Liu, J. Qiu, J. An, J. Yao, S. Zuo, B. Zhang, H. Xia, C. Li, Photocatalytic Oxidation of 5-Hydroxymethylfurfural Over Interfacial-Enhanced Ag/TiO<sub>2</sub> Under Visible Light Irradiation, *ChemSusChem.* 15 (2022). <https://doi.org/10.1002/cssc.202102158>.
- [116] J. Wen, J. Xie, X. Chen, X. Li, A review on g-C<sub>3</sub>N<sub>4</sub>-based photocatalysts, *Appl Surf Sci.* 391 (2017) 72–123. <https://doi.org/10.1016/j.apsusc.2016.07.030>.
- [117] J. Cui, X. Lu, M. Guo, M. Zhang, L. Sun, J. Xiong, R. Zhang, X. Li, Y. Qiao, D. Li, M. Guo, Z. Yu, Construction of a g-C<sub>3</sub>N<sub>4</sub>-driven photocatalytic system for boosted biomass-derived alcohol oxidation: a promising route towards sustainable biomass valorization, *Catal Sci Technol.* 13 (2023) 940–957. <https://doi.org/10.1039/d2cy01860h>.
- [118] Q. Wu, Y. He, H. Zhang, Z. Feng, Y. Wu, T. Wu, Photocatalytic selective oxidation of biomass-derived 5-hydroxymethylfurfural to 2,5-diformylfuran on metal-free g-C<sub>3</sub>N<sub>4</sub> under visible light irradiation, *Molecular Catalysis.* 436 (2017) 10–18. <https://doi.org/10.1016/j.mcat.2017.04.012>.
- [119] I. Krivtsov, E.I. García-López, G. Marcì, L. Palmisano, Z. Amghouz, J.R. García, S. Ordóñez, E. Díaz, Selective photocatalytic oxidation of 5-hydroxymethyl-2-furfural to 2,5-furandicarboxyaldehyde in aqueous suspension of g-C<sub>3</sub>N<sub>4</sub>, *Appl Catal B.* 204 (2017) 430–439. <https://doi.org/10.1016/j.apcatb.2016.11.049>.
- [120] M. Ilkaeva, I. Krivtsov, J.R. García, E. Díaz, S. Ordóñez, E.I. García-López, G. Marcì, L. Palmisano, M.I. Maldonado, S. Malato, Selective photocatalytic oxidation of 5-hydroxymethyl-2-furfural in aqueous suspension of polymeric carbon nitride and its adduct with H<sub>2</sub>O<sub>2</sub> in a solar pilot plant, *Catal Today.* 315 (2018) 138–148. <https://doi.org/10.1016/j.cattod.2018.03.013>.
- [121] S. Xu, P. Zhou, Z. Zhang, C. Yang, B. Zhang, K. Deng, S. Bottle, H. Zhu, Selective Oxidation of 5-Hydroxymethylfurfural to 2,5-Furandicarboxylic Acid Using O<sub>2</sub> and a Photocatalyst of Co-thioporphyrazine Bonded to g-C<sub>3</sub>N<sub>4</sub>, *J Am Chem Soc.* 139 (2017) 14775–14782. <https://doi.org/10.1021/jacs.7b08861>.

- [122] Y. Zhu, Y. Zhang, L. Cheng, M. Ismael, Z. Feng, Y. Wu, Novel application of g-C<sub>3</sub>N<sub>4</sub>/NaNbO<sub>3</sub> composite for photocatalytic selective oxidation of biomass-derived HMF to FFCA under visible light irradiation, *Advanced Powder Technology*. 31 (2020) 1148–1159. <https://doi.org/10.1016/j.apt.2019.12.040>.
- [123] H.F. Ye, R. Shi, X. Yang, W.F. Fu, Y. Chen, P-doped Zn<sub>x</sub>Cd<sub>1-x</sub>S solid solutions as photocatalysts for hydrogen evolution from water splitting coupled with photocatalytic oxidation of 5-hydroxymethylfurfural, *Appl Catal B*. 233 (2018) 70–79. <https://doi.org/10.1016/j.apcatb.2018.03.060>.
- [124] Q. Zhu, Y. Zhuang, H. Zhao, P. Zhan, C. Ren, C. Su, W. Ren, J. Zhang, D. Cai, P. Qin, 2,5-Diformylfuran production by photocatalytic selective oxidation of 5-hydroxymethylfurfural in water using MoS<sub>2</sub>/CdIn<sub>2</sub>S<sub>4</sub> flower-like heterojunctions, *Chin J Chem Eng*. 54 (2023) 180–191. <https://doi.org/10.1016/j.cjche.2022.04.018>.
- [125] S. Dhingra, T. Chhabra, V. Krishnan, C.M. Nagaraja, Visible-Light-Driven Selective Oxidation of Biomass-Derived HMF to DFF Coupled with H<sub>2</sub> Generation by Noble Metal-Free Zn<sub>0.5</sub>Cd<sub>0.5</sub>S/MnO<sub>2</sub> Heterostructures, *ACS Appl Energy Mater*. 3 (2020) 7138–7148. <https://doi.org/10.1021/acsaem.0c01189>.
- [126] M. Alfè, D. Spasiano, V. Gargiulo, G. Vitiello, R. Di Capua, R. Marotta, TiO<sub>2</sub>/graphene-like photocatalysts for selective oxidation of 3-pyridine-methanol to vitamin B<sub>3</sub> under UV/solar simulated radiation in aqueous solution at room conditions: The effect of morphology on catalyst performances, *Appl Catal A Gen*. 487 (2014) 91–99. <https://doi.org/10.1016/j.apcata.2014.09.002>.
- [127] S. Yurdakal, Ş.Ö. Yanar, S. Çetinkaya, O. Alagöz, P. Yalçın, L. Özcan, Green photocatalytic synthesis of vitamin B<sub>3</sub> by Pt loaded TiO<sub>2</sub> photocatalysts, *Appl Catal B*. 202 (2017) 500–508. <https://doi.org/10.1016/j.apcatb.2016.09.063>.
- [128] M. Bettoni, S. Meniconi, C. Rol, G. V. Sebastiani, Selective photocatalytic oxidation at TiO<sub>2</sub>/Ti anodes of 4-methoxybenzyl alcohol to the corresponding benzaldehyde in “green” conditions, *J Photochem Photobiol A Chem*. 222 (2011) 180–184. <https://doi.org/10.1016/j.jphotochem.2011.05.019>.
- [129] K. Fahlbusch, F. Hammerschmidt, J. Panten, W. Pickenhagen, D. Schatkowski, K. Bauer, D. Garbe, H. Surburg, *Flavors and Fragrances*, in: Ullmann’s Encyclopedia of Industrial Chemistry, Wiley, 2003. [https://doi.org/10.1002/14356007.a11\\_141](https://doi.org/10.1002/14356007.a11_141).
- [130] L. Özcan, S. Yurdakal, V. Augugliaro, V. Loddo, S. Palmas, G. Palmisano, L. Palmisano, Photoelectrocatalytic selective oxidation of 4-methoxybenzyl alcohol in water by TiO<sub>2</sub> supported on titanium anodes, *Appl Catal B*. 132–133 (2013) 535–542. <https://doi.org/10.1016/j.apcatb.2012.12.030>.
- [131] Z. Wu, J. Wang, Z. Zhou, G. Zhao, Highly selective aerobic oxidation of biomass alcohol to benzaldehyde by an: In situ doped Au/TiO<sub>2</sub> nanotube photonic crystal photoanode for simultaneous hydrogen production promotion, *J Mater Chem A Mater*. 5 (2017) 12407–12415. <https://doi.org/10.1039/c7ta03252h>.

- [132] J.C. Colmenares, R. Luque, Heterogeneous photocatalytic nanomaterials: Prospects and challenges in selective transformations of biomass-derived compounds, *Chem Soc Rev.* 43 (2014) 765–778. <https://doi.org/10.1039/c3cs60262a>.
- [133] C.R. Lhermitte, K. Sivula, Alternative Oxidation Reactions for Solar-Driven Fuel Production, *ACS Catal.* 9 (2019) 2007–2017. <https://doi.org/10.1021/acscatal.8b04565>.
- [134] Z. Zhou, Y.N. Xie, W. Zhu, H. Zhao, N. Yang, G. Zhao, Selective photoelectrocatalytic tuning of benzyl alcohol to benzaldehyde for enhanced hydrogen production, *Appl Catal B.* 286 (2021). <https://doi.org/10.1016/j.apcatb.2020.119868>.
- [135] C. Pulignani, C.A. Mesa, S.A.J. Hillman, T. Uekert, S. Giménez, J.R. Durrant, E. Reisner, Rational Design of Carbon Nitride Photoelectrodes with High Activity Toward Organic Oxidations, *Angewandte Chemie - International Edition.* 61 (2022). <https://doi.org/10.1002/anie.202211587>.
- [136] H.G. Cha, K.S. Choi, Combined biomass valorization and hydrogen production in a photoelectrochemical cell, *Nat Chem.* 7 (2015) 328–333. <https://doi.org/10.1038/nchem.2194>.
- [137] L. Özcan, P. Yalçın, O. Alagöz, S. Yurdakal, Selective photoelectrocatalytic oxidation of 5-(hydroxymethyl)-2-furaldehyde in water by using Pt loaded nanotube structure of TiO<sub>2</sub> on Ti photoanodes, *Catal Today.* 281 (2017) 205–213. <https://doi.org/10.1016/j.cattod.2016.07.024>.
- [138] C. Li, J. Li, L. Qin, P. Yang, D.G. Vlachos, Recent Advances in the Photocatalytic Conversion of Biomass-Derived Furanic Compounds, *ACS Catal.* 11 (2021) 11336–11359. <https://doi.org/10.1021/acscatal.1c02551>.
- [139] G. Totaro, L. Sisti, P. Marchese, M. Colonna, A. Romano, C. Gioia, M. Vannini, A. Celli, Current Advances in the Sustainable Conversion of 5-Hydroxymethylfurfural into 2,5-Furandicarboxylic Acid, *ChemSusChem.* 15 (2022). <https://doi.org/10.1002/cssc.202200501>.
- [140] H. Xu, X. Li, W. Hu, Z. Yu, H. Zhou, Y. Zhu, L. Lu, C. Si, Research Progress of Highly Efficient Noble Metal Catalysts for the Oxidation of 5-Hydroxymethylfurfural, *ChemSusChem.* 15 (2022). <https://doi.org/10.1002/cssc.202200352>.
- [141] S.K. Pahari, Y.T. Chen, In situ observation of photoelectrochemical water oxidation intermediates for selective biomass upgrading with simultaneous hydrogen production, *Chemical Engineering Journal.* 473 (2023). <https://doi.org/10.1016/j.cej.2023.145232>.
- [142] D.J. Chadderdon, L.P. Wu, Z.A. McGraw, M. Panthani, W. Li, Heterostructured Bismuth Vanadate/Cobalt Phosphate Photoelectrodes Promote TEMPO-Mediated Oxidation of 5-Hydroxymethylfurfural, *ChemElectroChem.* 6 (2019) 3387–3392. <https://doi.org/10.1002/celec.201900482>.
- [143] S. Yurdakal, S. Çetinkaya, M.B. Şarlak, L. Özcan, V. Loddo, L. Palmisano, Photoelectrocatalytic oxidation of 3-pyridinemethanol to 3-pyridinemethanal and vitamin B3 by TiO<sub>2</sub> nanotubes, *Catal Sci Technol.* 10 (2020) 124–137. <https://doi.org/10.1039/c9cy01583c>.



- [144] S. Yurdakal, S. Çetinkaya, L. Özcan, Ö. Gök, L. Palmisano, Partial photoelectrocatalytic oxidation of 3-pyridinemethanol by Pt, Au and Pd loaded TiO<sub>2</sub> nanotubes on Ti plate, *Catal Today*. 380 (2021) 248–258. <https://doi.org/10.1016/j.cattod.2020.11.003>.
- [145] D. Liu, J.C. Liu, W. Cai, J. Ma, H. Bin Yang, H. Xiao, J. Li, Y. Xiong, Y. Huang, B. Liu, Selective photoelectrochemical oxidation of glycerol to high value-added dihydroxyacetone, *Nat Commun*. 10 (2019). <https://doi.org/10.1038/s41467-019-09788-5>.
- [146] Z. Gu, X. An, R. Liu, L. Xiong, J. Tang, C. Hu, H. Liu, J. Qu, Interface-modulated nanojunction and microfluidic platform for photoelectrocatalytic chemicals upgrading, *Appl Catal B*. 282 (2021). <https://doi.org/10.1016/j.apcatb.2020.119541>.
- [147] S. Çetinkaya, G. Khamidov, L. Özcan, L. Palmisano, S. Yurdakal, Selective photoelectrocatalytic oxidation of glycerol by nanotube, nanobelt and nanosponge structured TiO<sub>2</sub> on Ti plates, *J Environ Chem Eng*. 10 (2022). <https://doi.org/10.1016/j.jece.2022.107210>.
- [148] C.M. Pecoraro, F. Di Franco, M. Bellardita, V. Loddo, M. Santamaria, Enhancing H<sub>2</sub> production rate in PGM-free photoelectrochemical cells by glycerol photo-oxidation, *Int J Hydrogen Energy*. (2023). <https://doi.org/10.1016/J.IJHYDENE.2023.08.011>.
- [149] Y. Jung, S. Kim, H. Choi, Y. Kim, J.B. Hwang, D. Lee, Y. Kim, J.C. Park, D.Y. Kim, S. Lee, Photoelectrochemical Selective Oxidation of Glycerol to Glyceraldehyde with Bi-Based Metal–Organic-Framework-Decorated WO<sub>3</sub> Photoanode, *Nanomaterials*. 13 (2023). <https://doi.org/10.3390/nano13101690>.
- [150] L. Luo, W. Chen, S.M. Xu, J. Yang, M. Li, H. Zhou, M. Xu, M. Shao, X. Kong, Z. Li, H. Duan, Selective Photoelectrocatalytic Glycerol Oxidation to Dihydroxyacetone via Enhanced Middle Hydroxyl Adsorption over a Bi<sub>2</sub>O<sub>3</sub>-Incorporated Catalyst, *J Am Chem Soc*. 144 (2022) 7720–7730. <https://doi.org/10.1021/jacs.2c00465>.
- [151] H. Tateno, S.Y. Chen, Y. Miseki, T. Nakajima, T. Mochizuki, K. Sayama, Photoelectrochemical Oxidation of Glycerol to Dihydroxyacetone Over an Acid-Resistant Ta:BiVO<sub>4</sub> Photoanode, *ACS Sustain Chem Eng*. 10 (2022) 7586–7594. <https://doi.org/10.1021/acssuschemeng.2c01282>.
- [152] Z. Tian, Y. Da, M. Wang, X. Dou, X. Cui, J. Chen, R. Jiang, S. Xi, B. Cui, Y. Luo, H. Yang, Y. Long, Y. Xiao, W. Chen, Selective photoelectrochemical oxidation of glucose to glucaric acid by single atom Pt decorated defective TiO<sub>2</sub>, *Nat Commun*. 14 (2023). <https://doi.org/10.1038/s41467-023-35875-9>.
- [153] Z. Zhao, M. Qu, M. Zhu, H. Shi, X. Luo, T. Guo, Q. Sun, L. Wang, H. Zheng, Crystal Facet-Modulated WO<sub>3</sub> Nanoplate Photoanode for Photoelectrochemical Glyoxal Semi-oxidation into Glyoxylic Acid, *ACS Appl Mater Interfaces*. 14 (2022) 48752–48761. <https://doi.org/10.1021/acsaami.2c14442>.
- [154] C.A. Mesa, A. Kafizas, L. Francàs, S.R. Pendlebury, E. Pastor, Y. Ma, F. Le Formal, M.T. Mayer, M. Grätzel, J.R. Durrant, Kinetics of Photoelectrochemical Oxidation of Methanol on Hematite Photoanodes, *J Am Chem Soc*. 139 (2017) 11537–11543. <https://doi.org/10.1021/jacs.7b05184>.

- [155] A.W. Harris, O. Yehezkeli, G.R. Hafenstine, A.P. Goodwin, J.N. Cha, Light-Driven Catalytic Upgrading of Butanol in a Biohybrid Photoelectrochemical System, *ACS Sustain Chem Eng.* 5 (2017) 8199–8204. <https://doi.org/10.1021/acssuschemeng.7b01849>.
- [156] D.S. Choi, J. Kim, F. Hollmann, C.B. Park, Solar-Assisted eBiorefinery: Photoelectrochemical Pairing of Oxyfunctionalization and Hydrogenation Reactions, *Angewandte Chemie - International Edition.* 59 (2020) 15886–15890. <https://doi.org/10.1002/anie.202006893>.
- [157] A. Hammer, M.A. Hiskey, G. Holl, T.M. Klapötke, K. Polborn, J. Stierstorfer, J.J. Weigand, Azidoformamidinium and guanidinium 5,5'-azotetrazolate salts, *Chemistry of Materials.* 17 (2005) 3784–3793. <https://doi.org/10.1021/cm050684f>.
- [158] R.P. Singh, R.D. Verma, D.T. Meshri, J.M. Shreeve, Energetic nitrogen-rich salts and ionic liquids, *Angewandte Chemie - International Edition.* 45 (2006) 3584–3601. <https://doi.org/10.1002/anie.200504236>.
- [159] H. He, J. Du, B. Wu, X. Duan, Y. Zhou, G. Ke, T. Huo, Q. Ren, L. Bian, F. Dong, Photoelectrochemical driving and clean synthesis of energetic salts of 5,5'-azotetrazolate at room temperature, *Green Chemistry.* 20 (2018) 3722–3726. <https://doi.org/10.1039/c8gc01663a>.
- [160] J. Huang, A. Liao, D. Yang, J. Wang, B. Wu, G. Ke, W. Yao, Y. Zhou, H. He, Magnetic field improved photoelectrochemical synthesis of 5,5'-azotetrazolate energetic salts and hydrogen in a hematite photoanode-based cell, *Electrochim Acta.* 330 (2020). <https://doi.org/10.1016/j.electacta.2019.135217>.
- [161] Y. Tang, B. Wu, H. He, C. Fu, J. Wang, K. Liu, G. Ke, Y. Zhou, Photoelectrochemical Driving and Simultaneous Synthesis of 3-pyridinecarboxylic Acid and Hydrogen in WO<sub>3</sub> Photoanode-Based Cell, *J Electrochem Soc.* 166 (2019) H662–H668. <https://doi.org/10.1149/2.0941913jes>.
- [162] S. Çetinkaya, L. Özcan, O. Alagöz, L. Palmisano, S. Yurdakal, Selective photoelectrocatalytic oxidation of 3-methylpyridine to vitamin B3 by WO<sub>3</sub> decorated nanotube-structured TiO<sub>2</sub>, *Chemical Communications.* 59 (2023) 5741–5744. <https://doi.org/10.1039/d3cc01394d>.